Institute of Space and Aeronautical Science University of Tokyo
Report No. 392, January 1965

Second-Order Supersonic Small Disturbance Theory

By

Keiichi KARASHIMA

Summary. A study of plane and axially symmetric supersonic flow is made for the approximate inviscid theory of such comparatively thick bodies that the linearized equation does not adequately predict an essential feature of flow. The second-order small disturbance equations are derived for plane and axially symmetric motions involving shock waves and the range of applicability is shown from order estimation of the error involved in the approximation.

For very high supersonic Mach numbers it is shown that the present approach is reduced to the first-order hypersonic small disturbance theory proposed by Van Dyke and, therefore, a single small disturbance theory may predict the flow at all supersonic speeds above the trasonic.

Several examples are numerically calculated for two-dimensional biconvex circular-arc airfoils, cones and a paraboloid-arc half-body of revolution with respect to their surface pressure distribution and initial shock wave curvature, etc., and compared with full solutions and other approximate solutions when available.

Experimental measurement of surface pressure distribution and observation of shape of the shock wave are made for a paraboloid-arc half-body of revolution with fineness ratio of 6.693 and for Mach numbers of 2, 3 and 8, and the results are compared with those of the present theory and others.

It is concluded that the present theory agrees well with the method of characteristics and the experimental results also confirm the present approach.

SYMBOLS

$(\bar{x}, \bar{r})$	non-dimensional Cartesian or cylindrical coordinates system normalized by length of the body
$(\bar{u}, \bar{v})$	components of local velocity vector
$\bar{\rho}$	density
$\bar{p}$	pressure
(x, r)	reduced coordinates system
(u, v)	reduced form of velocity components
ρ	reduced density
p	reduced pressure
M	free stream Mach number
β_s	local shock wave angle
δ	semi-vertex angle of body
τ	maximum slope of shock wave
τ_0	thickness of body

θ	conical parameter defined by r/x
$\bar{r}$	strained radial coordinate
$\bar{\theta}$	strained conical parameter
ψ	stream function
ω	entropy function
$S(x)$	shape function of shock wave
C_p	pressure coefficient
f, g, h, i	functions in series expansion for stream function
l, m	coefficients in series expansion of shock shape
$\omega_0, \omega_1, \omega_2$	coefficients in series expansion of ω
a_1, a_2, a_3	coefficients in differential equation (see Eq. (3.4.6))
g_1, g_2, g_3	coefficients in solution of g (see Eq. (3.4.10))
h_1, h_2, h_3, h_4	coefficients in solution of h (see Eq. (3.4.17))
i_1, i_2, i_3, i_4	coefficients in solution of i (see Eq. (3.4.19))
A, B, C, D, E, F, G, I	coefficients in differential equation (see Eq. (4.3.8) and Eq. (4.3.16)

Subscripts:

s	value at shock wave
b	value on the surface of body
o	value at the tip of pointed body of revolution
∞	value in free stream
$( )'$	derivative with respect to argument

1. Introduction

Most of the supersonic flows past plane or axially symmetric bodies with an attached shock wave can be solved numerically with required accuracy by use of the method of characteristics. However, if the flow properties in the disturbed field due to a body are small compared with those in the undisturbed flow, it may be expected that the small disturbance approximation will predict the flow field with ample accuracy. In this sense, in treating the supersonic flows past aerodynamic bodies with attached shock waves, there have been developed many simplified theories, which are based upon the assumption of small disturbance due to thin bodies.

The linearized theory [1], [2], which is the simplest form of all small disturbance theories, has been belived to be of practical value and often used to estimate the flow properties in the disturbed field. The basic assumption made in the linearized theory is in that the body is so thin that the shock wave can be replaced by isentropic compression waves. Although the body can be always chosen to be so thin that the linearization assumption is approximately valid, such a choice often seems to be very severe for practical use. For example, the

error in surface pressure coefficient for a plane wedge with semi-vertex angle of 15° and at Mach number of 2 is about 30 percents relative to the exact value.

In order to increase the accuracy of solution higher-order approximations have been developed, for example, by Lighthill [*3*] for plane flow and by Van Dyke [*4*] for axially symmetric flow, etc.. The assumption made in the shock-expansion method proposed originally by Lighthill [*3*] was proved to be reasonable by Eggers and Syvertson [*5*] by means of method of characteristics, even if the body thickness may be comparatively large. Thus the shock-expansion method seems to be most accurate and convenient of all approximate methods for plane flow, when it is used in estimation of the flow properties on the surface of the body with an atsached shock wave. However, in estimation of the flow properties in the disturbed field downstream of the shock wave, the same laborious work is necessary even for the shock-expansion method as will be required in the the characteristics net work.

Contrary to the shock-expansion method, the second-order theory proposed by Van Dyke [*4*] for axially symmetric flow was derived on the basis that all higher-oder terms in the fundamental equation are considered to be perturbations from basic linearized equation. Being essentially based upon the assumption of potential flow, this theory together with the linearized theory seems to grow increasingly inaccurate as either the body thickness or the free stream Mach number increases.

On the other hand, the flow in the region of leading edge or pointed apex of curved bodies has been investigated in detail by many authors with particular emphasis on the initial surface pressure gradient and shock wave curvature. Among these works Kraus [*6*] presented detailed charts for two-dimensional curved airfoils by use of method of characteristics and Shen and Lin [*7*] investigated the flow in the neighborhood of the sharp nose of a body of revolution by means of a perturbation scheme. Having not been made for entire flow field, these analyses seem to have significance as being the first-step in clarifying the general problem of flow past an arbitrary body with an attached shock wave. It must, however, be noted that the first-order solution in Shen and Lin's analysis shows a logarithmic singularity at the initial semi-vertex angle and the initial surface pressure gradient becomes infinite even for regular body shape. This result seems to be unrealistic, since the method of characteristics does not indicate such a singularity.

More recently, Van Dyke [*8*] proposed a well-refined hypersonic small disturbance theory, in which the non-linearity in the fundamental equations and shock wave conditions is considered to be an essential feature of the flow. In his analysis he gave a criterion for first-order hypersonic small disturbance flow and derived a useful similarity law, which was shown to be further combined with the supersonic simirarity law [*8*], [*9*]. Moreover, this theory seems to be of practical value in the sense that it does not indicate such a singularity as was presented by Shen and Lin. However, since the basic assumption made in this theory becomes severe for comparatively low supersonic Mach numbers, the theory seems

to be inaccurate as Mach number decreases.

As is well known, the degree of disturbance downstream of the shock wave is directly associated with the strength of the shock wave. For low supersonic Mach numbers the shock wave slope is not so small compared with unity even if the body thickness is small. For such flow the first-order theory, which is developed in such a way that the full solution is expanded in a power series with respect to a representative value of the shock wave slope, becomes inaccurate. Therefore, a higher-order approximation must be made in order to obtain better agreement with the full solution.

Present paper has a purpose to give an analytical approach to the second-order plane and axially symmetric supersonic small disturbance flows. With particular emphasis on presenting an unified theory for plane and axially symmetric motions involving shock waves at all supersonic Mach numbers above the transonic, the second-order small disturbance equations are derived on the basis of appropriate assumptions and applied to several simple examples. The fact that the analytical method used in the present approach is the same as Van Dyke developed in the first-order small disturbance theory indicates, therefore, significance that the present approach corresponds to a second-order theory relative to Van Dyke's first-order theory at hypersonic Mach numbers as well as being an extension of the hypersonic theory to comparatively thick bodies at low supersonic Mach numbers. In this sense, the present theory may be regarded as an unified, approximate theory for predicting both supersonic and hypersonic flows past plane and axially symmetric bodies with attached shock waves.

In order to confirm the present theory an experimental measurement of surface pressure was made for a paraboloid-arc half-body of revolution and the results are compared with present theory, method of characteristics and other approximate theories.

2. Basic Assumptions and Equations

Consider a steady supersonic flow involving an oblique shock wave which emanates from tip of a body. Since viscous no-slip condition requires large perturbation of flow properties near the surface of the body, viscosity and heat conduction must be primarily neglected in the small disturbance theory. Therefore, the flow is assumed to be inviscid and non-conductive. The body is assumed to be thin in the sense that the streamwise slope of its surface is everywhere small compared with unity. This assumption is, in turn, interpreted into a statement that the body curvature must be of the same order as maximum slope of the surface. The so-called hypersonic is not particularly distinguished from the supersonic in the present approach.

There are two representative parameters which are used as measures of degree of disturbance in flow field downstream of a shock wave. The one is body thickness and the another is shock wave slope. From a mathematical point of view, all small disturbance methods which are developed for vanishing by thin bodies

may be regarded as an asymptotic form in series expansion of the full theory with respect to body thickness. Thus, the first-order theory is obtained as the leading term of the series, in which the body thickness is assumed to be very small compared with unity.

The basic assumption made in Van Dyke's first-order hypersonic small disturbance theory thus derived is in that the terms of order of $\tau\delta$ are negligible compared with unity, where τ and δ denote shock wave slope and characteristic body thickness such as maximum flow deflection angle through shock wave, respectively. This assumption seems to be reasonable for very high Mach numbers, since τ becomes of order of δ, so that $\tau\delta=O(\delta^2)$.

For comparatively low supersonic Mach numbers, however, τ is not so small compared with unity, even if the body may be thin. As a result $\tau\delta$ becomes of order of δ and, consequently, the first-order theory is increasingly inaccurate as Mach number decreases. In order to reduce the error in approximation even for the ordinary supersonic, higher-order terms in the series must be retained. Therefore, the second-order small disturbance flows may have such an assumption as

$$\tau\delta<1\,,\qquad \frac{\delta^3}{\tau}\ll 1\,. \tag{2.1}$$

This indicates that the terms of order of δ^3/τ are negligible in the present approach. For very high Mach numbers, however, it becomes

$$\frac{\delta^3}{\tau}\longrightarrow\delta^2\,, \tag{2.2}$$

so that the error in this second-order theory grows to the same order as that in Van Dyke's theory in limiting case when Mach number tends to infinity.

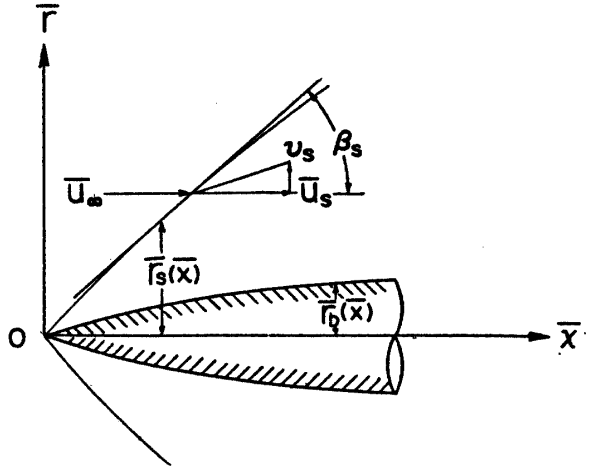

FIGURE 1. Plane or axially symmetric body.

Let the origin of a Cartesian or cylindrical coordinates system be taken at the leading edge of the airfoil for plane flow or at the pointed apex of the body of revolution for axially symmetric flow, $\bar{x}$-axis being aligned with the free stream direction, and $\bar{r}$-axis being normal to $\bar{x}$-axis (see Fig. 1). If the shape of the shock wave is given as

$$\bar{r}_s=\tau S(\bar{x})\,, \tag{2.3}$$

$$\frac{d\bar{r}_s}{d\bar{x}}=\tan\beta_s=\tau S'(\bar{x})\,, \tag{2.4}$$

then, the flow properties just aft of the shock wave are

$$\frac{\bar{u}_s}{\bar{u}_\infty}=1+\frac{2}{(\gamma+1)M^2}-\frac{2}{\gamma+1}\frac{\tau^2S'^2}{1+\tau^2S'^2}\,, \tag{2.5a}$$

$$\frac{\bar{v}_s}{\bar{u}_\infty}=\frac{2}{\gamma+1}\frac{\tau S'}{1+\tau^2S'^2}\left(1-\frac{1+\tau^2S'^2}{M^2\tau^2S^2}\right), \tag{2.5b}$$

$$\frac{\bar{\rho}_s}{\bar{\rho}_\infty}=\frac{(\gamma+1)M^2\tau^2S'^2}{(\gamma-1)M^2\tau^2S'^2+2(1+\tau^2S'^2)}\,, \tag{2.5c}$$

$$\frac{\bar{p}_s}{\bar{p}_\infty}=1+\frac{2\gamma}{\gamma+1}\left(\frac{M^2\tau^2S^2}{1+\tau^2S'^2}-1\right), \tag{2.5d}$$

where β_s, $\bar{u}$, $\bar{v}$, $\bar{p}$ and $\bar{\rho}$ denote local shock wave angle, components of local velocity vector in $\bar{x}$- and $\bar{r}$-directions, density and pressure, respectively, and subscripts ∞ and s indicate conditions in free stream and just downstream of the shock wave, respectively. τ is the maximum slope of the shock wave, which is, in general, given at its root for conventional convex body, so that $S'(\bar{x})$ does not exceed unity. Another boundary condition is given on the body surface as

(tangency) $$\bar{v}=\bar{u}\frac{d\bar{r}_b}{d\bar{x}} \qquad \text{ar} \quad \bar{r}=\bar{r}_b(\bar{x})\,, \tag{2.6}$$

where $\bar{r}_b(\bar{x})$ denotes body surface.

As is seen in Eqs. (2.5a) to (2.5d), the boundary conditions at the shock wave consist of terms of M^{-2}, $M^2\tau^2$ and τ^2. This fact indicates that the flow does no longer be predicted by a single parametric representation (similarity parameter) as is done by $\beta\tau_0$ in the linearized theory or by $M\tau_0$ in Van Dyke's hypersonic small disturbance theory, where $\beta=\sqrt{M^2-1}$.

The differential equations which govern the flow field are

(continuity) $$(\bar{\rho}\bar{u})_{\bar{x}}+(\bar{\rho}\bar{v})_{\bar{r}}+\sigma\frac{\bar{\rho}\bar{v}}{\bar{r}}=0\,, \tag{2.7a}$$

(x-momentum) $$\bar{u}\bar{u}_{\bar{x}}+\bar{v}\bar{u}_{\bar{r}}+\frac{1}{\bar{\rho}}\bar{p}_{\bar{x}}=0\,, \tag{2.7b}$$

(r-momentum) $$\bar{u}\bar{v}_{\bar{x}}+\bar{v}\bar{v}_{\bar{r}}+\frac{1}{\bar{\rho}}\bar{p}_{\bar{r}}=0\,, \tag{2.7c}$$

(entropy) $$\bar{u}\left(\frac{\bar{p}}{\bar{\rho}^\gamma}\right)_{\bar{x}}+\bar{v}\left(\frac{\bar{p}}{\bar{\rho}^\gamma}\right)_{\bar{r}}=0\,, \tag{2.7d}$$

where

$\sigma=0$ for plane flow

$\sigma=1$ for axially symmetric flow

and where subscripts indicate differentiation and γ is the ratio of specific heats.

Introducing a transformation of independent and dependent variables such as

$$\left.\begin{aligned} x&=\bar{x}\,,\\ r&=\frac{1}{\tau}\bar{r}\,, \end{aligned}\right\} \tag{2.8a}$$

$$\begin{aligned} &\bar{u}=\bar{u}_\infty\{a+\tau^2u(x,r)\}\,, \qquad a=1+\frac{2}{(\gamma+1)M^2}\,,\\ &\bar{v}=\bar{u}_\infty\tau\cdot v(x,r)\,,\\ &\bar{\rho}=\bar{\rho}_\infty\rho(x,r)\,,\\ &\bar{p}=\bar{p}_\infty\gamma M^2\tau^2p(x,r)\,, \end{aligned} \tag{2.8b}$$

and rewriting Eqs. (2.7a) to (2.7d), then gives

(continuity) $$\{\rho(a+\tau^2u)\}_x+(\rho v)_r+\sigma\frac{\rho v}{r}=0\,, \tag{2.9a}$$

(x-momentum) $$(a+\tau^2u)u_x+vu_r+\frac{1}{\rho}p_x=0\,, \tag{2.9b}$$

(r-momentum) $$(a+\tau^2u)v_x+vv_r+\frac{1}{\rho}p_r=0\,, \tag{2.9c}$$

(entropy) $$(a+\tau^2u)\left(\frac{p}{\rho^\gamma}\right)_x+v\left(\frac{p}{\rho^\gamma}\right)_r=0\,. \tag{2.9d}$$

The conditions along shock wave and on the body surface are written, respectively, as

$$u_s=-\frac{2}{\gamma+1}\frac{S'^2}{1+\tau^2S'^2}\,, \tag{2.10a}$$

$$v_s=\frac{2}{\gamma+1}\frac{S'}{1+\tau^2S'^2}\left(1-\frac{1+\tau^2S'^2}{M^2\tau^2S'^2}\right), \tag{2.10b}$$

$$\rho_s=\frac{(\gamma+1)M^2\tau^2S'^2}{(\gamma-1)M^2\tau^2S'^2+2(1+\tau^2S'^2)}\,, \tag{2.10c}$$

$$p_s=\frac{2\gamma M^2\tau^2S'^2-(\gamma-1)(1+\tau^2S'^2)}{\gamma(\gamma+1)M^2\tau^2(1+\tau^2S'^2)}\,, \tag{2.10d}$$

(tangency) $$v=(a+\tau^2u)\frac{dr_b}{dx} \qquad \text{at} \quad r=r_b(x)\,. \tag{2.11}$$

3. Plane Flow Problem

3.1. *Fundamental Equation*

Continuity equation may be accounted by for introducing a stream function ψ,

$$\psi_x=-\rho v\,, \qquad \psi_r=\rho(a+\tau^2u)\,. \tag{3.1.1}$$

Then, entropy equation predicts that p/ρ^γ is a function of only ψ. This clearly indicates the fact that entropy is constant along stream lines between shock waves. Thus, a new entropy function ω is defined as

$$\frac{p}{\rho^\gamma}=\omega(\psi)\,. \tag{3.1.2}$$

Rewriting Eqs. (2.9b) and (2.9c) by use of Eqs. (3.1.1) and (3.1.2), and eliminating u, v and p, one obtains

$$\psi_r^2\psi_{xx}-2\psi_x\psi_r\psi_{xr}+\psi_x^2\psi_{rr}=\gamma\omega\rho^r\psi_r\rho_r+\omega'\rho^{r+1}\psi_r^2+\tau^2(\gamma\omega\rho^r\psi_x\rho_x+\omega'\rho^{r+1}\psi_x^2)\,, \tag{3.1.3}$$

where

$$\omega'=\frac{d\omega}{d\psi}\,. \tag{3.1.4}$$

ρ and its derivatives which appear explicitly in right-hand side of the above equation can be eliminated by use of Bernoulli's law in principle, since the system of equations has, at present, been completely closed because of four unknowns (u, v, p, ρ) to be determined and four equations (Eqs. (2.9a) to (2.9d)). Bernoulli's equation is written as

$$\psi_r^2+\tau^2\psi_x^2+\frac{2\gamma}{\gamma-1}\tau^2\omega\rho^{r+1}=\left(1+\frac{2}{(\gamma-1)M^2}\right)\rho^2\,. \tag{3.1.5}$$

However, it is impossible to obtain an analytical solution of Eq. (3.1.5) for ρ, so that it is required to find out another expression for ρ to use instead of Eq. (3.1.5). Although Bernoulli's equation has a physical meaning of energy conservation along a stream line, the new expression for ρ, be it exact or approximate, is not always necessary to have a definite physical meaning but may be only mathematical to express a quantitative relation between ρ and ψ in the flow field.

This relation can be derived from a consideration that the flow behind a shock wave is supposed to consist of a basic, uniform wedge field upon which is superimposed a perturbation field due to body curvature. Therefore, the velocity components u, v in the flow field are also assumed to consist of two parts. The one is appropriate to the basic wedge flow and the another is due to the body curvature such as

$$\left.\begin{aligned} u(x, r)&=u_w+u_p(x, r)\,,\\ v(x, r)&=v_w+v_p(x, r)\,, \end{aligned}\right\} \tag{3.1.6}$$

where u_w and v_w denote reduced velocity components appropriate to the basic wedge flow, which are given, respectively, as

$$u_w=-\frac{2}{\gamma+1}\,\frac{1}{1+\tau^2}\,, \tag{3.1.7}$$

$$v_w=\frac{2}{\gamma+1}\,\frac{1}{1+\tau^2}\left(1-\frac{1+\tau^2}{M^2\tau^2}\right), \tag{3.1.8}$$

and u_p and v_p are those due to body curvature.

On the other hand, from the definition of stream function, following expression is obtained:

$$\psi_r-\tau^2\psi_x=\rho\left[1+\frac{2}{(\gamma+1)M^2}+\tau^2(u+v)\right]. \tag{3.1.9}$$

Substitution of Eq. (3.1.6) into Eq. (3.1.9) gives

$$\psi_r-\tau^2\psi_x=\rho[1+\tau^2(u_p+v_p)]\,. \tag{3.1.10}$$

Hence, if the second term in the bracket is assumed to be very small compared with unity, the above equation may be reduced to a simple form such as

$$\rho=\psi_r-\tau^2\psi_x\,. \tag{3.1.11}$$

Here the validity of the above assumption must be confirmed. It is readily clear that Eq. (3.1.11) is exact for wedge flows, because both u_p and v_p vanish. For flows past curved airfoils order of disturbance in the flow field may be evaluated from that just behind the leading edge shock wave, that is

$$u_p(x, r)+v_p(x, r)=0\{(u_{p_s}+v_{p_s})\}\,,$$

where subscript s indicates condition just aft of the shock wave. Since Mach waves that emanate from the airfoil surface interact with the shock wave, local shock wave slope τ_s is changed by $\Delta\tau$ from its basis wedge value τ;

$$\begin{cases}\tau_s=\tau+\Delta\tau\,,\\ \tau_s=\tan\beta_s\,, \qquad \tau=\tan\beta_w\,,\end{cases}$$

where β_s and β_w denote local shock wave angle and its basic wedge value, respectively. The change in local shock wave slope $\Delta\tau$ may be of order of shock wave curvature K_s

$$\Delta\tau=K_s x=O(K_s)\,.$$

On the other hand, the change in velocity components due to $\Delta\tau$ is expressed by use of shock wave relations as

$$\begin{aligned}u_{p_s}+v_{p_s}&=\frac{2\{M^2\tau^2-(1+\tau^2)\}\tau}{(\gamma+1)M^2\tau^2(1+\tau^2)\tau}\Delta\tau\\ &\doteqdot\frac{\delta\cdot\Delta\tau}{\tau^2(1+\tau^2)}\,,\end{aligned}$$

where

$$\begin{aligned}M^2\tau^2-(1+\tau^2)&=\frac{1}{2}\tau\delta[\{(\gamma+1)+(\gamma-1)\tau^2\}M^2+2(1+\tau^2)]\\ &\doteqdot\frac{\gamma+1}{2}M^2\tau\delta\,,\\ \delta&=\tan\theta_w\,,\end{aligned}$$

and where θ_w is semi-angle of the basic wedge. The above relation can be rewritten by use of body curvature K_b as

$$u_{p_s}+v_{p_s}=O\left(\frac{\delta^2}{\tau^2}\,\frac{K_s}{K_b}\right),$$

in which the assumption, $K_b=O(\delta)$, has been used. The ratio of shock to body curvature can be estimated from the result given by Kraus [6] by use of method of characteristics.

$$\frac{K_s}{K_b}=\frac{\gamma+1}{4\cos(\beta_w-\theta_w)}\left[\frac{1-\dfrac{\tan^2(\beta_w-\theta_w)}{\tan^2\mu_2}}{\dfrac{\tan^2(\beta_w-\theta_w)}{\tan^2\mu_2}+\dfrac{1}{2}\left\{\dfrac{\cos^2\mu_2}{\cos^2(\beta_w-\theta_w)}+\dfrac{1}{M^2\sin^2\beta_w}\right\}}\right],$$

where μ_2 is Mach angle just aft of the shock wave. Order estimation of the above equation gives (see Appendix 1)

$$\frac{K_s}{K_b}=O\left(\frac{\delta}{\tau}\right).$$

From these results the second term in the bracket of Eq. (3.1.10) may be found to be of order of

$$\tau^2(u_p+v_p)=O\left(\frac{\delta^3}{\tau}\right)\ll 1,$$

and is negligible from the basic assumption (2.1). Thus, the validity of Eq. (3.3.11) is confirmed and the order of error involved in the equation is $O(\delta^3/\tau)$. By use of Eq. (3.1.11), Eq. (3.1.3) is expressed as

$$\begin{aligned}&\psi_r^2\psi_{xx}-2\psi_x\psi_r\psi_{xr}+\psi_x^2\psi_{rr}\\&=\psi_r^{\gamma+1}(\gamma\omega\psi_{rr}+\omega'\psi_r^2)+\tau^2\psi_r^{\gamma}(\gamma\omega\psi_x\psi_{xr}+\omega'\psi_r\psi_x^2\\&\quad-\gamma^2\omega\psi_x\psi_{rr}-\gamma\omega\psi_r\psi_{xr}-\omega'(\gamma+1)\psi_x\psi_r^2)\end{aligned}\tag{3.1.12}$$

where terms of order of δ^3/τ and $\tau^2\delta^2$ have been neglected in the above equation (see Note, p. 49).

3.2. *Range of Applicability of Eq. (3.1.12)*

In the last section the fundamental equation has been derived with an additional assumption that $\tau^2\delta^2$ is very small compared with unity. This assumption is clearly valid for high Mach numbers because $\tau^2\delta^2\to\delta^4$. For ordinary supersonic Mach numbers, however, it increases rapidly as Mach number decreases. Nevertheless, the present theory may give a wider range of applicability than Van Dyke's first-order theory, since x-momentum equation (Eq. (2.7b)), which has been dropped in the first-order theory, is of order of $\tau\delta$. In this sense, it is of interest to clarify the range in which Eq. (3.1.12) is applicable.

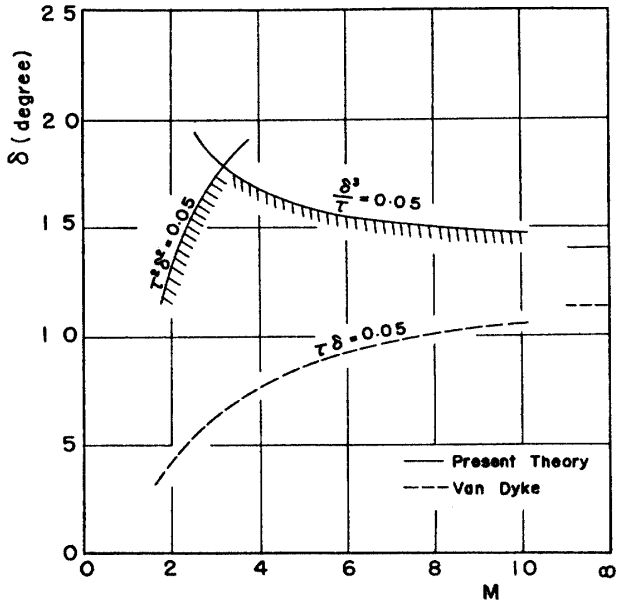

FIGURE 2. Range of applicability of the present theory for plane flow, Eq. (3.1.12).

In Fig. 2 is presented an example for variation of semi-vertex angle of the airfoils with free stream Mach number, in which δ^3/τ and $\tau^2\delta^2$ are used as parameters. In the figure the hatched region bounded by lines having $\delta^3/\tau=\tau^2\delta^2=0.05$ indicates the domain in which Eq. (3.1.12) may be applicable within 5 percent error. A boundary having $\tau\delta=0.05$ is also shown for comparison. The figure shows that the present theory may be applicable to comparatively thick airfoils at all supersonic Mach numbers above the transonic.

3.3. *Application to Plane Wedge*

As the simplest example, consider a supersonic flow past a wedge of semi-vertex angle δ. In this case the flow field is conical, so that stream function and shock wave shape have the form

$$\psi(x, r)=xf(\theta)\,, \tag{3.3.1}$$

$$r_s=S(x)=x\,, \tag{3.3.2}$$

respectively, where θ is a conical parameter defined by

$$\theta=\frac{\bar{r}}{\tau\bar{x}}=\frac{r}{x}\,. \tag{3.3.3}$$

Hence, the shock wave conditions are given at $\theta=\theta_s=1$. The flow field downstream of the shock wave is irroiational and uniform, so that the entropy function is constant everywhere and is expressed as

$$\omega(\psi)=\omega_0=\frac{2\gamma M^2\tau^2-(\gamma-1)(1+\tau^2)}{\gamma(\gamma+1)M^2\tau^2(1+\tau^2)}\left[\frac{(\gamma-1)M^2\tau^2+2(1+\tau^2)}{(\gamma+1)M^2\tau^2}\right]^{\gamma}. \tag{3.3.4}$$

Substitution of Eq. (3.3.1) into Eq. (3.1.12) leads to the following ordinary differential equation for $f(\theta)$;

$$f''=0\,. \tag{3.3.5}$$

Conditions at the shock wave are obtained from Eqs. (2.10a) to (2.10d) as

$$\left.\begin{aligned} &f(1)=1\,,\\ &f'(1)=\frac{\tau^2}{1+\tau^2}\,\frac{\{(\gamma+1)+(\gamma-1)\tau^2\}M^2+2(1+\tau^2)}{(\gamma-1)M^2\tau^2+2(1+\tau^2)}\,. \end{aligned}\right\} \tag{3.3.6}$$

The solution to Eq. (3.3.5) is, therefore, given by

$$f(\theta)=\bar{A}_0\theta-\bar{B}_0\,, \tag{3.3.7}$$

where

$$\left.\begin{aligned} &\bar{A}_0=f'(1)\,,\\ &\bar{B}_0=-[f(1)-f'(1)]\,. \end{aligned}\right\} \tag{3.3.8}$$

Requiring $f(\theta)$ to vanish at the surface θ_b gives the ratio of wedge to shock wave slope

$$\theta_b=\frac{\delta}{\tau}=\frac{\bar{B}_0}{\bar{A}_0}\,. \tag{3.3.9}$$

The pressure coefficient C_p is defined by the equation

$$C_p=\frac{\bar{p}-\bar{p}_\infty}{{}^1/_2\bar{\rho}_\infty\bar{u}_\infty^2}\,, \tag{3.3.10}$$

and is expressed by use of transformation of the variables as

$$C_p=2\tau^2\left(\omega\rho^\gamma-\frac{1}{\gamma M^2\tau^2}\right), \tag{3.3.11}$$

Therefore, the surface pressure coefficient for the wedge flow is given as

$$C_p=\frac{4\{M^2\tau^2-(1+\tau^2)\}}{(\gamma+1)(1+\tau^2)M^2}. \tag{3.3.12}$$

It must be noted that Eq. (3.1.11) gives an exact relation between ρ and stream function for the wedge flow. Moreover, the boundary conditions are also exact. These facts together with a result that Eq. (3.3.5) does not include any term with τ lead to the statement that the present approach gives exact solution for the plane wedge flow.

3.4. *Application to Convex Airfoils*

Consider a supersonic flow past a convex airfoil with an attached shock wave (see Fig. 1). In this case of flow pattern the expansion waves that emanate from the airfoil surface interact with the shock wave and weaken it to incline more and more to the free stream direction. The flow field downstream of the shock wave is, therefore, no longer irrotational and change in entropy of each stream line must be taken into consideration.

This problem can be treated by perturbation from the wedge flow as done by Van Dyke [8] in such a way that the flow behind the shock wave will consist of a uniform field upon which is superimposed a perturbation field due to body curvature. Hence, the flow properties along each ray from the vertex will have constant values associated with the initial slope of the body plus linear variations proportional to the initial curvature, together with higer variations if necessary. Thus, the shock wave shape and the stream function may be written, respectively, in the forms

$$r_s=S(x)=x-\frac{1}{2}lx^2-\frac{1}{3}mx^3-\cdots, \tag{3.4.1}$$

$$\psi(x,r)=xf(\theta)-lx^2g(\theta)-x^3\{mh(\theta)+l^2i(\theta)\}-\cdots. \tag{3.4.2}$$

In the same way the entropy function ω can be expressed in the form

$$\omega(\psi)=\omega_0\{1-\omega_1l\psi-\omega_2m\psi^2-\cdots\}. \tag{3.4.3a}$$

By use of Eq. (3.4.2) the above equation is rewritten as

$$\omega(\psi)=\omega_0[1-\omega_1lxf(\theta)-x^2\{\omega_2mf^2(\theta)-\omega_1l^2g(\theta)\}\cdots]. \tag{3.4.3b}$$

The conditions just behind the shock wave are found to be given by

$$(\psi_r)_s=\bar{A}_0+\bar{A}_1lx+(\bar{A}_2l^2+\bar{A}_1m)x^2+\cdots, \tag{3.4.4a}$$

$$(-\psi_x)_s=\bar{B}_0+\bar{B}_1lx+(\bar{B}_2l^2+\bar{B}_1m)x^2+\cdots, \tag{3.4.4b}$$

where subscript s denotes condition along shock wave, and

$$\bar{A}_0=\frac{\tau^2}{1+\tau^2}\frac{\{(\gamma+1)+(\gamma-1)\tau^2\}M^2+2(1+\tau^2)}{(\gamma-1)M^2\tau^2+2(1+\tau^2)},$$

$$\bar{B}_0=\frac{2}{1+\tau^2}\frac{M^2\tau^2-(1+\tau^2)}{(\gamma-1)M^2\tau^2+2(1+\tau^2)},$$

$$\bar{A}_1=-\left[\frac{4\tau^2}{1+\tau^2}\frac{\{(\gamma+1)+(\gamma-1)\tau^2\}M^2+2(1+\tau^2)}{\{(\gamma-1)M^2\tau^2+2(1+\tau^2)\}^2}-\frac{4\tau^2}{(1+\tau^2)^2}\frac{M^2\tau^2}{(\gamma-1)M^2\tau^2+2(1+\tau^2)}\right],$$

$$\bar{B}_1=-2\left[\frac{M^2\tau^2-(1+\tau^2)}{1+\tau^2}\frac{2-(\gamma-1)M^2\tau^2-2\tau^2}{\{(\gamma-1)M^2\tau^2+2(1+\tau^2)\}^2}+\frac{2}{(1+\tau^2)^2}\frac{M^2\tau^2}{(\gamma-1)M^2\tau^2+2(1+\tau^2)}\right],$$

$$\bar{A}_2=-\frac{2\tau^2\{3(\gamma-1)M^2\tau^2+6\tau^2-2\}}{\{(\gamma-1)M^2\tau^2+2(1+\tau^2)\}^3}\frac{\{(\gamma+1)+(\gamma-1)\tau^2\}M^2+2(1+\tau^2)}{1+\tau^2}$$
$$-\frac{16M^2\tau^4}{(1+\tau^2)^2\{(\gamma-1)M^2\tau^2+2(1+\tau^2)\}^2}-\frac{2M^2\tau^2(1-3\tau^2)}{(1+\tau^2)^3\{(\gamma-1)M^2\tau^2+2(1+\tau^2)\}},$$

$$\bar{B}_2=-\frac{2(\gamma+1)M^2\tau^2}{1+\tau^2}\frac{3(\gamma-1)M^2\tau^2+6\tau^2-2}{\{(\gamma-1)M^2\tau^2+2(1+\tau^2)\}^3}$$
$$+\frac{4(\gamma+1)M^2\tau^2(1-\tau^2)}{(+\tau^2)^2\{(\gamma-1)M^2\tau^2+2(1+\tau^2)\}^2}-\frac{2\tau^2(3-\tau^2)\{M^2\tau^2-(1+\tau^2)\}}{(1+\tau^2)^3\{(\gamma-1)M^2\tau^2+2(1+\tau^2)\}}. \quad (3.4.4c)$$

Since the stream function along the shock wave is given by $\psi_s=r_s$, Eq. (3.4.3a) can be expressed along the shock wave as

$$\omega(\psi_s)=\omega_s=\omega_0\left[1-\omega_1 lx-\left(\omega_2 m-\frac{1}{2}\omega_1 l^2\right)x^2-\cdots\right].$$

On the other hand, from the shock conditions ω_s is found to be

$$\omega_s=\omega_0[1-\omega_1 lx-(\omega_1 m-\alpha l^2)x^2-\cdots],$$

where

$$\omega_1=\frac{4\gamma(\gamma-1)\{M^2\tau^2-(1+\tau^2)\}^2}{(1+\tau^2)\{2\gamma M^2\tau^2-(\gamma-1)(1+\tau^2)\}\{(\gamma-1)M^2\tau^2+2(1+\tau^2)\}},$$

$$\alpha=\frac{2\gamma M^2\tau^2(1-3\tau^2)}{(1+\tau^2)^2\{2\gamma M^2\tau^2-(\gamma-1)(1+\tau^2)\}}+\frac{6\gamma}{(\gamma-1)M^2\tau^2+2(+\tau^2)}$$
$$-\frac{16\gamma^2M^2\tau^2}{(1+\tau^2)\{2\gamma M^2\tau^2-(\gamma-1)(1+\tau^2)\}\{\gamma-1)M^2\tau^2+2(1+\tau^2)\}}$$
$$+\frac{8\gamma(\gamma-1)}{\{(\gamma-1)M^2\tau^2+2(1+\tau^2)\}^2}, \quad (3.4.4d)$$

and where ω_0 has been given by Eq. (3.3.4). ω_2 is obtained by comparing the above two equations for ω_s as

$$\omega_2=\omega_1-\left(\alpha-\frac{1}{2}\omega_1\right)\frac{l^2}{m}. \quad (3.4.5)$$

Substituting Eqs. (3.4.2) and (3.4.3b) into Eq. (3.1.12) and equating like powers of x yields for f, g, h and i the linear ordinary differential equations, respectively. Equation for f is quite the same as is given by Eq. (3.3.5) as well as its boundary conditions corresponding to the basic wedge flow.

Equation for g, when simplified by use of Eq. (3.3.5), has a form

$$[f^2-\gamma\omega_0 f'^{\gamma+1}+\tau^2\gamma\omega_0 f'^{\gamma}\{(f-\theta f')\theta+\gamma(f-\theta f')-\theta f'\}]g''$$
$$-[2ff'+\tau^2\gamma\omega_0 f'^{\gamma}\{f-\theta f'-f'\}]g'+2f'^2 g=\omega_0\omega_1 f'^{\gamma+3}$$
$$+\tau^2\omega_0\omega_1 f'^{\gamma+1}(f-\theta f')(f-\theta f'-f').$$

With the aid of Eq. (3.3.7) the above equation can be more simplified as

$$(a_1\theta^2-a_2\theta+a_3)g''-(2a_1\theta-a_2)g'+2a_1 g=c, \tag{3.4.6}$$

where

$$\left.\begin{aligned} a_1&=\bar{A}_0^2,\\ a_2&=2\bar{A}_0\bar{B}_0+\tau^2\gamma\omega_0\bar{A}_0^{\gamma}(\bar{A}_0+\bar{B}_0),\\ a_3&=\bar{B}_0^2-\gamma\omega_0\bar{A}_0^{\gamma+1}-\tau^2\gamma^2\omega_0\bar{A}_0^{\gamma}\bar{B}_0,\\ c&=\omega_0\omega_1\bar{A}_0^{\gamma+1}\{\bar{A}_0^2+\tau^2\bar{B}_0(\bar{A}_0+\bar{B}_0)\}. \end{aligned}\right\} \tag{3.4.7}$$

At the shock wave the conical parameter θ_s becomes

$$\theta_s=\frac{r_s}{x}=1-\frac{1}{2}lx-\frac{1}{3}mx^2-\cdots, \tag{3.4.8}$$

so that Taylor expansion of ψ_x and ψ_r at the shock wave and comparison with Eqs. (3.4.4a) and (3.4.4b) lead to as boundary conditions on g (see Appendix 2)

$$\left.\begin{aligned} g(1)&=-\frac{1}{2}\bar{B}_0,\\ g'(1)&=-\bar{A}_1. \end{aligned}\right\} \tag{3.4.9}$$

The solution to Eq. (3.4.6) can easily be found to be

$$g(\theta)=g_1\theta^2+g_2\theta+g_3, \tag{3.4.10}$$

where

$$\left.\begin{aligned} g_1&=\frac{1}{\Delta}[2a_1\{g'(1)-g(1)\}-a_2 g'(1)+c],\\ g_2&=\frac{2}{\Delta}[(a_3-a_1)g'(1)+2a_1 g(1)-c],\\ g_3&=\frac{1}{\Delta}[-a_2 g'(1)+2(a_2-a_3)\{g'(1)-g(1)\}+c],\\ \Delta&=2(a_1-a_2+a_3). \end{aligned}\right\} \tag{3.4.11}$$

Equations for $h(\theta)$ and $i(\theta)$, which are simplified with the aid of Eqs. (3.3.7) and (3.4.10), are obtained, respectively, in the forms

$$(a_1\theta^2-a_2\theta+a_3)h''-2(2a_1\theta-a_2)h'+6a_1 h=2c(\bar{A}_0\theta-\bar{B}_0), \tag{3.4.12}$$
$$(a_1\theta^2-a_2\theta+a_3)i''-2(2a_1\theta-a_2)i'+6a_1 i=-b_0\theta+b_1, \tag{3.4.13}$$

where

$$b_0=2\bar{A}_0(g_2^2-4g_1g_3)+2\omega_0\bar{A}_0^{\gamma}g_1\{2\gamma(\gamma+1)g_1+(2\gamma+3)\omega_1\bar{A}_0^2\}$$
$$+\tau^2\omega_0\bar{A}_0^{\gamma-1}[\gamma g_2(\bar{A}_0 g_2-2\gamma\bar{B}_0 g_1)+\omega_1\bar{A}_0\bar{B}_0\{2(\gamma+1)\bar{B}_0 g_1-(\gamma+2)\bar{A}_0 g_2\}]$$
$$-2\tau^2\gamma\omega_0\bar{A}_0^{\gamma-1}g_1[\gamma(\bar{A}_0 g_2-2\gamma\bar{B}_0 g_1)+(\gamma+1)\bar{A}_0 g_2]$$
$$+\tau^2\omega_0\omega_1\bar{A}_0^{\gamma+1}[2(\gamma^2+\gamma+2)\bar{B}_0 g_1-(\gamma+1)\bar{A}_0 g_2]$$

$$+2\omega_0\left(\alpha-\frac{1}{2}\omega_1\right)\bar{A}_0^{\gamma+2}[\bar{A}_0^2+\tau^2\bar{B}_0(\bar{A}_0+\bar{B}_0)]\,, \tag{3.4.14a}$$

$$\begin{aligned}b_1=&2\bar{B}_0(g_2^2-4g_1g_3)-2\gamma\omega_0\bar{A}_0^{\gamma}g_1\{(\gamma+1)g_2-\omega_1\bar{A}_0\bar{B}_0\}-(\gamma+3)\omega_0\omega_1\bar{A}_0^{\gamma+2}g_2\\&-\tau^2\omega_0\bar{A}_0^{\gamma-1}[\gamma g_2(2\bar{A}_0g_3-\gamma\bar{B}_0g_2)+\omega_1\bar{A}_0\bar{B}_0\{(\gamma+2)\bar{B}_0g_2-4\bar{A}_0g_3\}]\\&+\tau^2\gamma\omega_0\bar{A}_0^{\gamma-1}g_2\{2\gamma(2\bar{A}_0g_3-\gamma\bar{B}_0g_2)+(\gamma+1)\bar{A}_0g_2\}\\&+2\tau^2\omega_0\omega_1\bar{A}_0^{\gamma}\{\gamma^2\bar{B}_0^2g_1-(\gamma+1)\bar{A}_0\bar{B}_0g_2-\bar{A}_0^2g_3\}\\&+2\omega_0\left(\alpha-\frac{1}{2}\omega_1\right)\bar{A}_0^{\gamma+1}\bar{B}_0[\bar{A}_0^2+\tau^2\bar{B}_0(\bar{A}_0+\bar{B}_0)]\,.\end{aligned} \tag{3.4.14b}$$

The boundary conditions are given, respectively, as

$$\left.\begin{aligned}h(1)&=-\frac{1}{3}\bar{B}_0\,,\\h'(1)&=-\bar{A}_1\,,\end{aligned}\right\} \tag{3.4.15}$$

$$\left.\begin{aligned}i(1)&=\frac{1}{3}\left(\bar{B}_2-\bar{A}_2-\frac{1}{2}\bar{A}_1\right),\\i'(1)&=g_1-\bar{A}_2\,.\end{aligned}\right\} \tag{3.4.16}$$

The solution to Eq. (3.4.12) is easily found to have the form

$$h(\theta)=h_1\theta^3+h_2\theta^2+h_3\theta+h_4\,. \tag{3.4.17}$$

Substituting Eq. (3.4.17) into Eq. (3.4.12) and equating like powers of θ, then gives two equations indicating a linear combination of the coefficients, h_i ($i=1, 2, 3, 4$). The other two equations for h_i are obtained from the boundary conditions. Thus, the all coefficients in Eq. (3.4.17) are determined by solving the simultaneous equations for h_i;

$$\left.\begin{aligned}3a_3h_1+a_2h_2+a_3h_3\qquad&=c\bar{A}_0\,,\\a_3h_2+a_2h_3+3a_1h_4&=-c\bar{B}_0\,,\\h_1+\ h_2+\ h_3+\ h_4&=h(1)\,,\\3h_1+\ 2h_2+\ h_3\qquad&=h'(1)\,.\end{aligned}\right\} \tag{3.4.18}$$

In quite the same way the solution to Eq. (3.4.13) can be obtained as

$$i(\theta)=i_1\theta^3+i_2\theta^2+i_3\theta+i_4\,, \tag{3.4.19}$$

where

$$\left.\begin{aligned}3a_3i_1+a_2i_2+a_1i_3\qquad&=-\frac{1}{2}b_0\,,\\a_3i_2+a_2i_3+3a_1i_4&=\frac{1}{2}b_1\,,\\i_1+\ i_2+\ i_3+\ i_4&=i(1)\,,\\3i_1+\ 2i_2+\ i_3\qquad&=i'(1)\,.\end{aligned}\right\} \tag{3.4.20}$$

Body surface is determined by vanishing of the stream function. Hence,

$$\begin{aligned}&(\bar{A}_0\theta_b-\bar{B}_0)-lx(g_1\theta_b^2+g_2\theta_b+g_3)-mx^2(h_1\theta_b^3+h_2\theta_b^2+h_3\theta_b+h_4)\\&-l^2x^2(i_1\theta_b^3+i_2\theta_b^2+i_3\theta_b+i_4)-\cdots=0\,,\end{aligned}$$

where θ_b denotes conical parameter for the body surface and is a function of x only. Taylor expansion of the above equation with respect to x yields for θ_b an expression

$$\begin{aligned}\theta_b=&\frac{\bar{B}_0}{\bar{A}_0}+\frac{1}{\bar{A}_0^3}(\bar{B}_0^2g_1+\bar{A}_0\bar{B}_0g_2+\bar{A}_0^2g_3)lx\\&+\frac{1}{\bar{A}_0^4}(h_1\bar{B}_0^3+h_2\bar{A}_0\bar{B}_0^2+h_3\bar{A}_{00}^2+h_4\bar{A}_0^3)mx^2\\&+\frac{1}{\bar{A}_0^5}[(\bar{A}_0g_2+2\bar{B}_0g_1)(\bar{A}_0^2g_3+\bar{A}_0\bar{B}_0g_2+\bar{B}_0^2g_1)\\&+\bar{A}_0(i_1\bar{B}_0^3+i_2\bar{B}_0^2\bar{A}_0+i_3\bar{A}_0^2\bar{B}_0+i_4\bar{A}_0^3)]l^2x^2+\cdots.\end{aligned}\tag{3.4.21}$$

Although l and m, etc., still remain unknown at the present stage of analysis, they can be determined by the given body shape. Thus, the plane problem can be solved completely.

3.5. *Biconvex Circular-Arc Airfoils*

In order to confirm the accuracy of the present approach numerical calculations were made for several biconvex circular-arc airfoils as simple examples. The body shape is given by

$$\theta_b=\frac{2\tau_0}{\tau}(1-x)\,.\tag{3.5.1}$$

By comparing Eq. (3.5.1) with Eq. (3.4.21) l and m are found to be

$$\frac{\bar{B}_0}{\bar{A}_0}=\frac{2\tau_0}{\tau}=(\theta_b)_{x=0}=\theta_0\,,\tag{3.5.2}$$

$$l=\frac{-\bar{A}_0^2\bar{B}_0}{\bar{A}_0^2g_3+\bar{A}_0\bar{B}_0g_2+\bar{B}_0^2g_1}\,,\tag{3.5.3}$$

$$m=-\frac{(\bar{A}_0g_2+2\bar{B}_0g_1)(\bar{A}_0^2g_3+\bar{A}_0\bar{B}_0g_2+\bar{B}_0^2g_1)+\bar{A}_0(i_1\bar{B}_0^3+i_2\bar{A}_0\bar{B}_0^2+i_3\bar{A}_0^2\bar{B}_0+i_4\bar{A}_0^3)}{\bar{A}_0(h_1\bar{B}_0^3+h_2\bar{A}_0\bar{B}_0^2+h_3\bar{A}_0^2\bar{B}+h_4\bar{A}_0^3}\times l^2\,.\tag{3.5.4}$$

Initial ratio of shock to body curvature is given by the equation

$$\frac{K_s}{K_b}=\frac{l\tau}{4\tau_0}\,,\tag{3.5.5}$$

and the initial slope of surface pressure coefficient is given by the equation

$$\left(\frac{1}{K_b}\frac{dC_p}{dx}\right)_{x=0}=-\frac{\gamma\omega_0}{2\tau_0}\tau^2\left(\rho_b^{\gamma-1}\frac{d\rho_b}{dx}\right)_{x=0}\,,\tag{3.5.6}$$

where

$$\left.\begin{aligned}\rho_b(0)&=\bar{A}_0(1+\tau^2\theta_0)\,,\\\left(\frac{d\rho_b}{dx}\right)_{x=0}&=-\{(2g_1\theta_0+g_2)-\tau^2(g_2\theta_0+2g_3)\}l\,.\end{aligned}\right\}\tag{5.5.7}$$

Figs. 3a to 3c show the variation of initial ratio of shock to body curvature with semi-vertex angle at Mach numbers of 2, 3 and 5, respectively. The results from method of characteristics calculated by Kraus [6] and from hypersonic

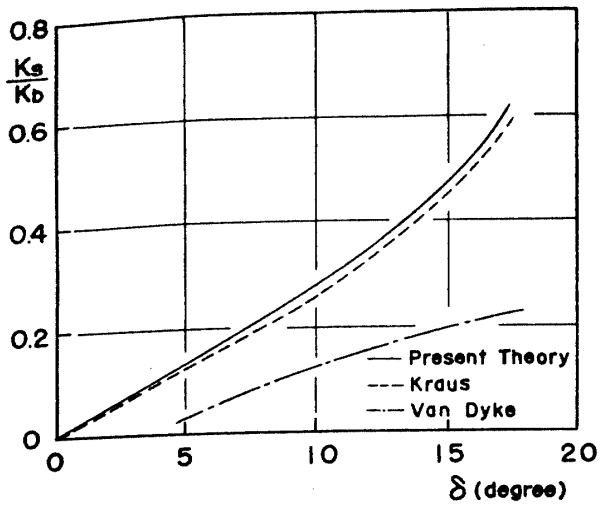

FIGURE 3a. Initial ratio of shock to body curvature for plane body, $M=2$.

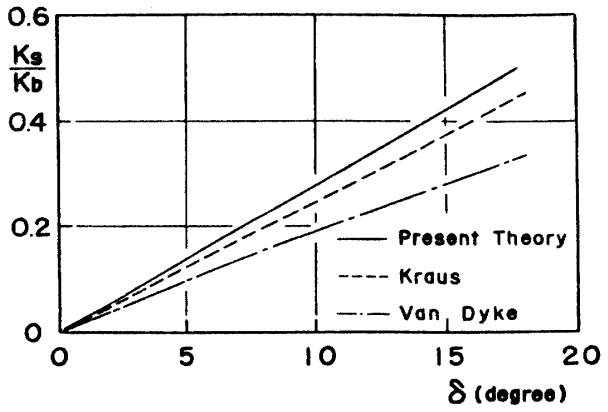

FIGURE 3b. Initial ratio of shock to body curvature for plane body, $M=3$.

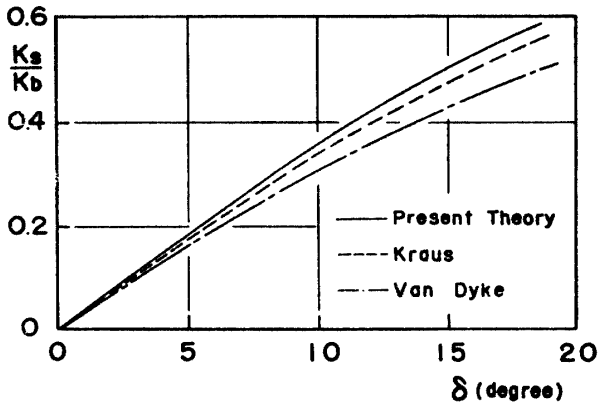

FIGURE 3c. Initial ratio of shock to body curvature for plane body, $M=5$.

small disturbance theory are shown in each figure for comparison. It is found that the present theory has better agreement with the method of characteristics than the hypersonic small disturbance theory which becomes increasingly inaccurate as Mach number decreases.

In Figs. 4a to 4c is presented the initial slope of the surface pressure coefficient at Mach numbers of 2, 3 and 5, respectively, and the results from method of characteristics [*6*] and from hypersonic small disturbance theory [*8*] are also presented in each figure for comparison. The agreement between present theory and method of characteristics is very good.

Figs. 5a to 5c show the surface pressure distribution for biconvex circular-arc airfoils with thickness-chord ratios of 0.05, 0.10 and 0.15, respectively, and at Mach number of 2. The surface pressure distributions for the same airfoils and at Mach numbers of 3 and 5 are shown, respectively, in Figs. 6a to 6c and in Figs. 7a to 7c. The results from the shock-expansion method and the linearized theory are also presented in each figure for comparison.

It must be noted here that the present theory should primarily be compared with the method of characteristics. However, Eggers and Syvertson [*5*] tried to make

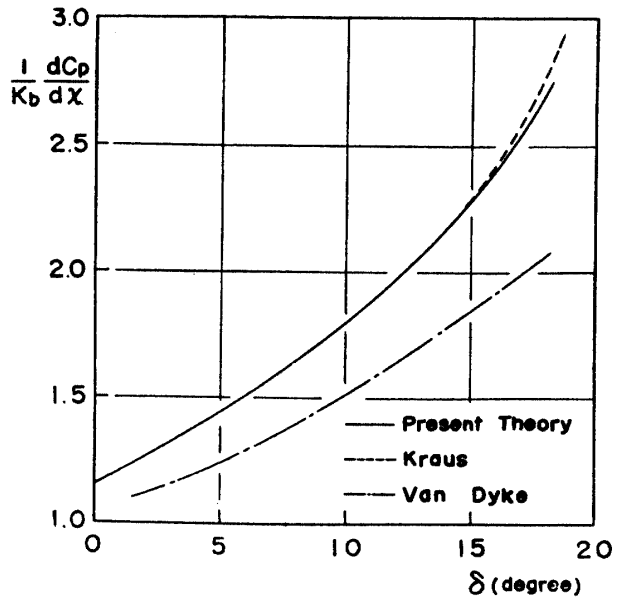

FIGURE 4a. Initial pressure gradient on plane body, $M=2$.

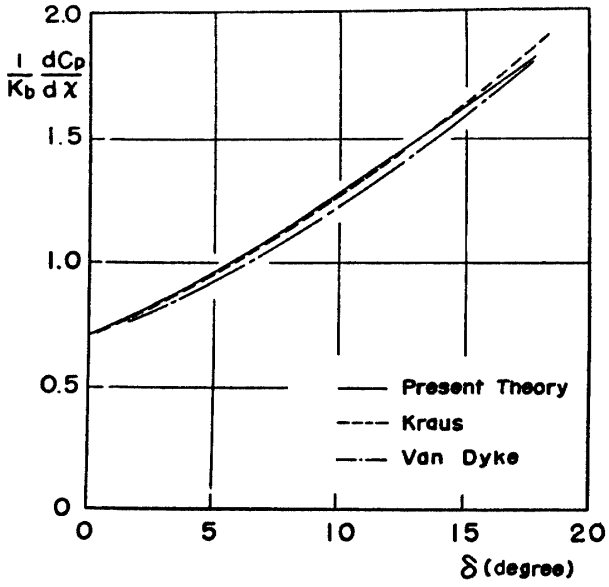

FIGURE 4b. Initial pressure gradient on plane body, $M=3$.

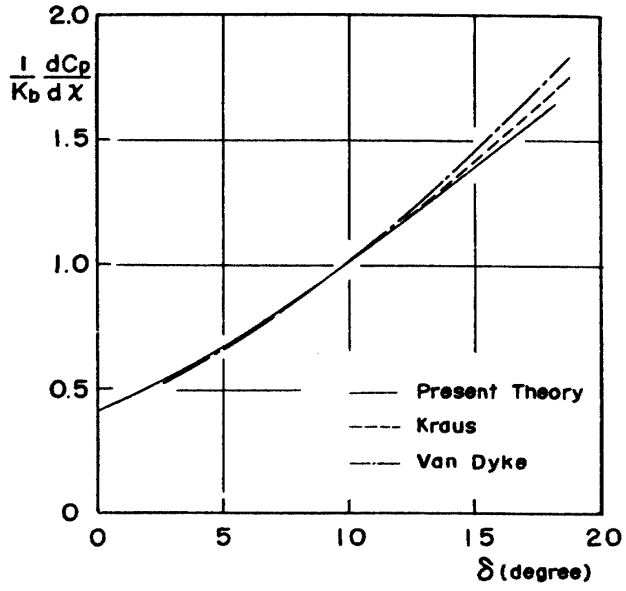

FIGURE 4c. Initial pressure gradient on plane body, $M=5$.

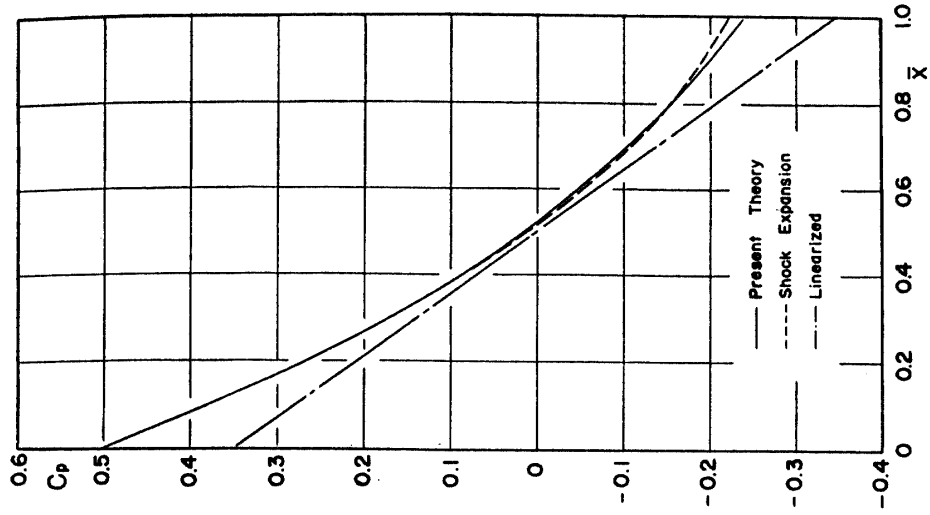

FIGURE 5c. Surface pressure distribution on biconvex circular-arc airfoil, $M=2, \tau_0=0.15$.

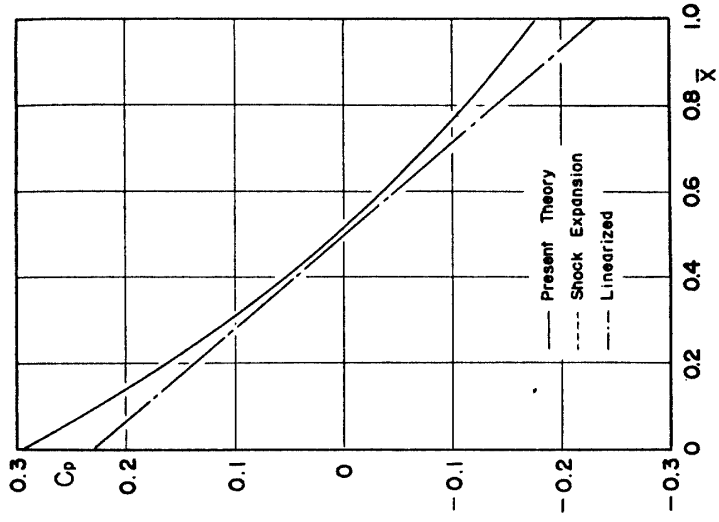

FIGURE 5b. Surface pressure distribution on biconvex circular-arc airfoil, $M=2, \tau_0=0.10$.

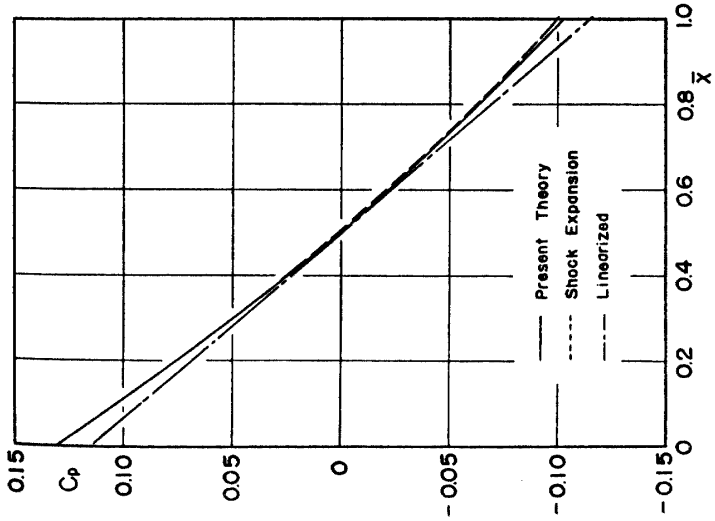

FIGURE 5a. Surface pressure distribution on biconvex circular-arc airfoil, $M=2, \tau_0=0.05$.

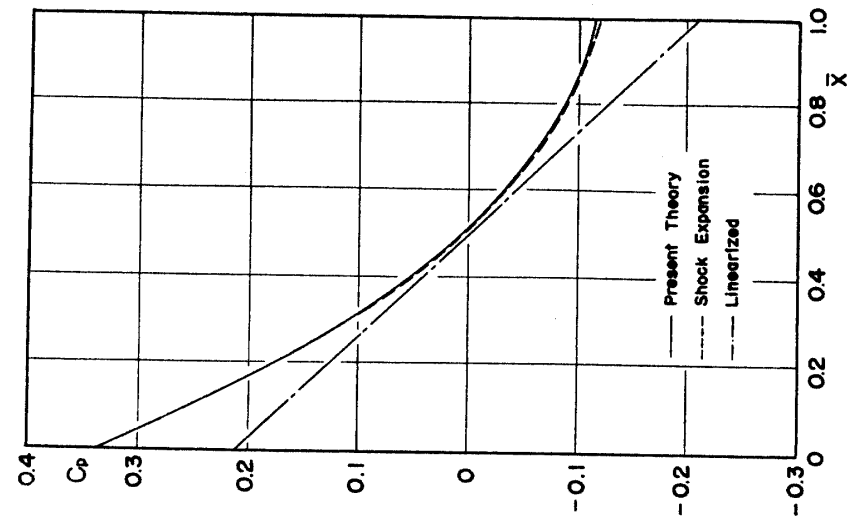

FIGURE 6c. Surface pressure distribution on biconvex circular-arc airfoil, $M=3$, $\tau_0=0.15$.

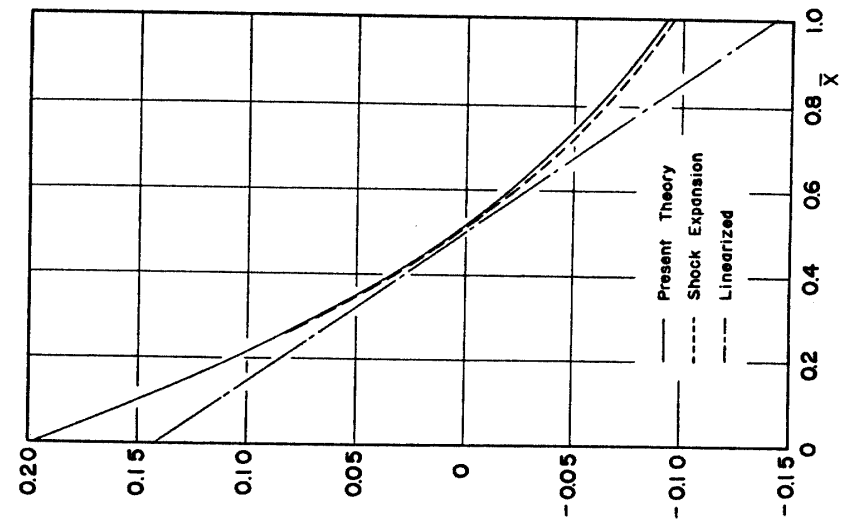

FIGURE 6b. Surface pressure distribution on biconvex circular-arc airfoil, $M=3$, $\tau_0=0.10$.

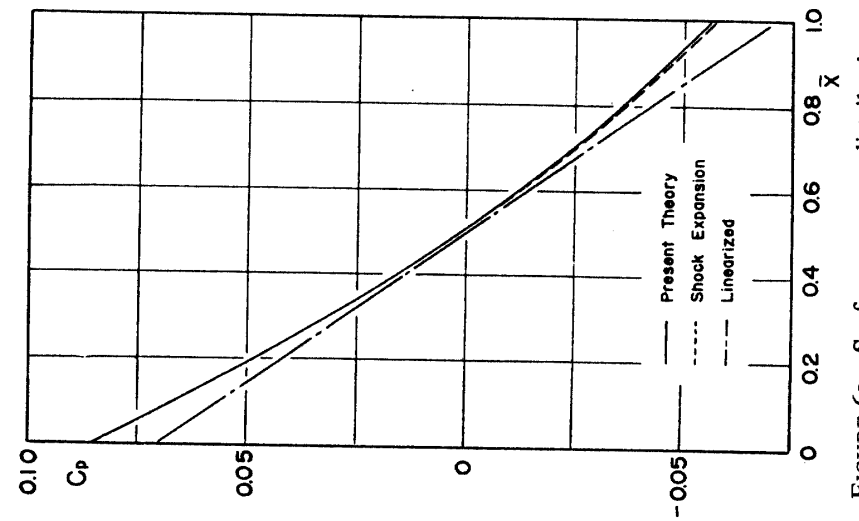

FIGURE 6a. Surface pressure distribution on biconvex circular-arc airfoil, $M=3$, $\tau_0=0.05$.

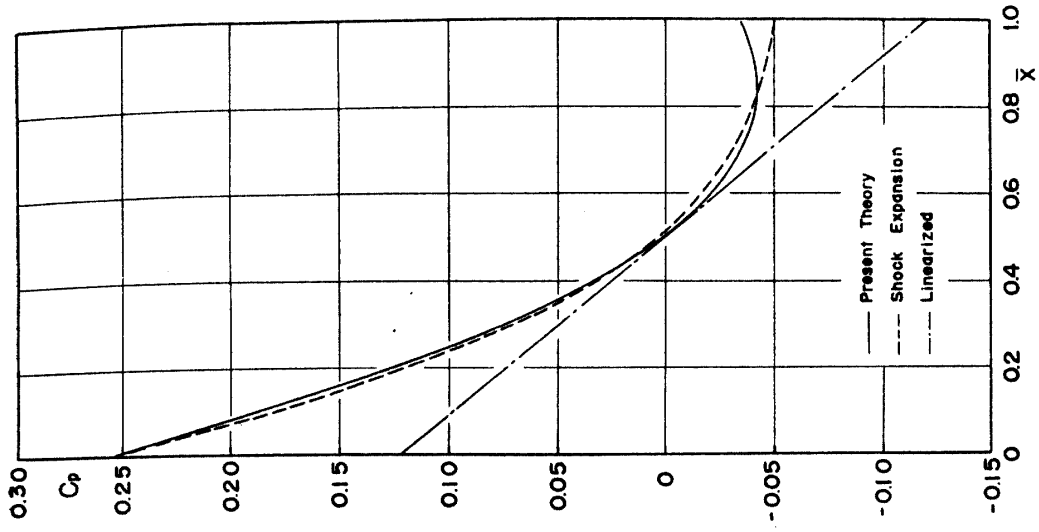

FIGURE 7c. Surface pressure distribution on biconvex circular-arc airfoil, $M=5$, $\tau_0=0.15$.

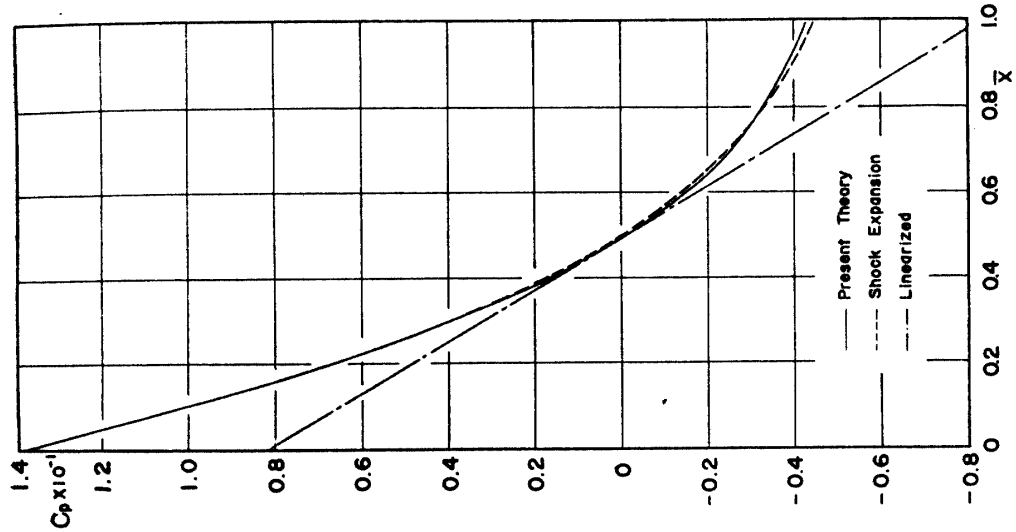

FIGURE 7b. Surface pressure distribution on biconvex circular-arc airfoil, $M=5$, $\tau_0=0.10$.

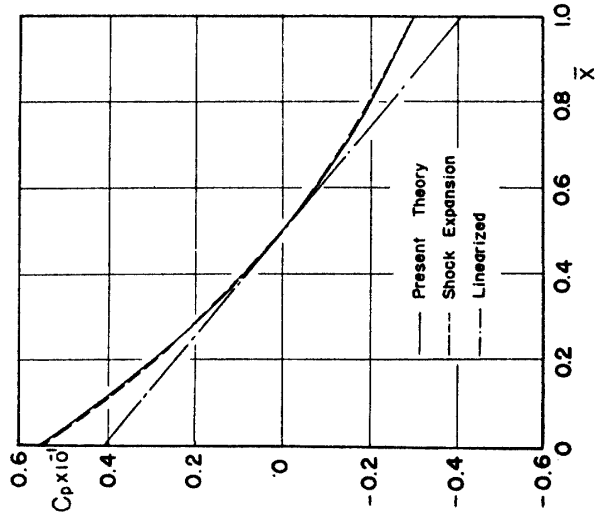

FIGURE 7a. Surface pressure distribution on biconvex circular-arc airfoil, $M=5$, $\tau_0=0.05$.

an over-all check on the shock-expansion method and revealed the fact that there is no apparent difference between the pressure distributions given by the method of characteristics and the shock-expansion method up to a Mach number of 10, above which the latter method predicts pressures that are slightly low downstream of the leading edge, becoming progressively lower with increasing Mach number. This can be interpreted into the statement that almost all of an incident disturbance emanating on the surface of the airfoil is generally absorbed in the shock

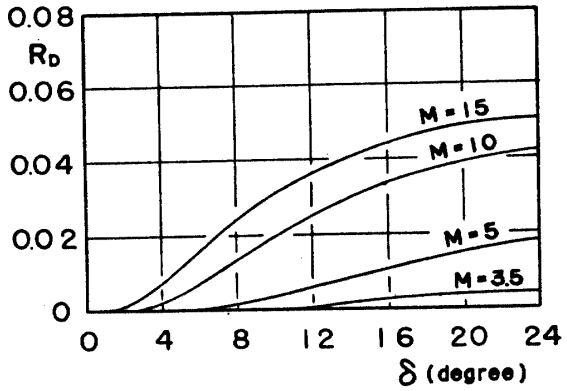

FIGURE 8. Variation of disturbance strength ratio behind an oblique shock wave with flow deflection angle δ.

wave. In Fig. 8 is presented the "disturbance strength ratio R_D" calculated by Eggers and Syvertson [5] by use of the method of characteristics as a reference. It is defined as the ratio of pressure gradient along a characteristic of the first family C_1 to that along the second family C_2 at the shock wave such as

$$R_D=-\frac{\partial p}{\partial c_1}\Big/\frac{\partial p}{\partial c_2}. \tag{3.5.8}$$

The fiure shows that the disturbance strength ratio is very small, thus giving an evidence that the flow field downstream of the shock wave can be considered, with ample accuracy, to be a region of simple wave.

Since the characteristics net-work is very much laborious, the present theory is compared with the shock-expansion method for the reason just mentioned above. As is seen in Figs. 5a to 7c, the present theory agrees well with the shock-expansion method, which, in turn, with the method of characteristics. However, in the case of thickness-chord ratio of 0.15 and at Mach number of 5, the present theory seems to deviate from the shock-expansion method in the region near the trailing edge. This does not arise from essential inaccuracy of the present theory, so that the deviation will be improved by taking more higher terms in series expansion of the stream function, Eq. (3.4.2).

4. Axially Symmetric Flow Problem

4.1. *Fundamental Equation*

For the axially symmetric flows past pointed bodies of revolution the continuity equation, Eq. (2.9a), may be accounted for by introducing a stream function ψ

and the entropy function $\omega(\psi)$ such as

$$\psi_x=-r\rho v\,,\qquad \psi_r=r\rho(\alpha+\tau^2 u)\,, \tag{4.1.1}$$

$$\omega(\psi)=\frac{p}{\rho^\gamma}\,. \tag{4.1.2}$$

The entropy equation is then automatically satisfied by the stream function and entropy function. The mathematical expression indicating a relation between ρ and ψ in the flow field can be obtained from an analogous discussion as has been made in Section 3.1. The flow downstream of a shock wave attached to a body of revolution (see Fig. 1) is assumed to consist of a basic conical field upon which is superimposed a disturbance field due to body curvature. Therefore, the velocity components u, v in the flow field are also considered to consist of two parts. The one is appropriate to the basic conical flow and the another is due to the body curvature. Hence,

$$\left.\begin{aligned} u(x,r)&=u_c(x,r)+u_p(x,r)\,,\\ v(x,r)&=v_c(x,r)+v_p(x,r)\,, \end{aligned}\right\} \tag{4.1.3}$$

where u_c and v_c denote reduced velocity components appropriate to the basic conical field and u_p and v_p are those due to the body curvature.

From the definition of stream function it is obtained that

$$\frac{\psi_r-\tau^2\psi_x}{r}=\rho\{a+\tau^2(u+v)\}\,.$$

Substitution of Eq. (4.1.3) into the above equation leads to

$$\frac{\psi_r-\tau^2\psi_x}{r}=\rho\left\{1+\frac{2}{(\gamma+1)M^2}+\tau^2(u_c+v_c)+\tau^2(u_p+v_p)\right\}. \tag{4.1.4}$$

The third term in bracket of right-hand side of the above equation may be of order of δ^3/τ from an order estimation analogous to the plane flow and, hence, negligible. However, contrary to the plane problem, the velocity components appropriate to the basic conical flow are not constant in this case, so that an order estimation must be made for the second term in bracket of Eq. (4.1.4), which can be made by use of conical theory proposed by Taylor and Maccoll (11).

The conical flow has a similar solution which is analytic everywhere in the flow field, so that an series expansion of velocity components about shock wave is possible such as

$$\begin{aligned} u_c+v_c=u_{c_s}+v_{c_s}&-\left\{\left(\frac{du_c}{d\theta}\right)_s+\left(\frac{dv_c}{d\theta}\right)_s\right\}(1-\theta)\\ &+\frac{1}{2}\left\{\left(\frac{d^2u_c}{d\theta^2}\right)_s-\left(\frac{d^2v_c}{d\theta^2}\right)_s\right\}(1-\theta)^2+O\{(1-\theta)^3\}\,, \end{aligned}$$

where θ denotes a conical variable defined by r/x, so that the shock wave is given by $\theta=1$, and where

$$u_{c_s}+v_{c_s}=-\frac{2}{(\gamma+1)M^2\tau^2}\,.$$

With the aid of the conical theory, coefficient of the second term of the above

series is easily found to vanish and the coefficient of the third term is expressed as

$$\left(\frac{d^2u_c}{d\theta^2}\right)_s+\left(\frac{d^2v_c}{d\theta^2}\right)_s=\left(\frac{2}{\gamma+1}\right)^2\left(\frac{1}{1+\tau^2}\right)^2\frac{2\gamma M^2\tau^2-(\gamma-1)(1+\tau^2)}{2M^2\tau^2}.$$

Therefore,

$$\begin{aligned}&1+\frac{2}{(\gamma+1)M^2}+\tau^2(u_c+v_c)\\&=1+\frac{1}{2}\left\{\frac{2\tau}{(\gamma+1)(1+\tau^2)}\right\}^2\frac{2\gamma M^2\tau^2-(\gamma-1)(1+\tau^2)}{2M^2\tau^2}(1-\theta)^2+O\{(1-\theta)^3\}.\end{aligned}\quad(4.1.5)$$

The maximum value of the second term in right-hand side of the above equation is given on the cone surface $\theta=\theta_b=\delta/\tau$, so that

$$\frac{1}{2}\left\{\frac{2\tau}{(\gamma+1)(1+\tau^2)}\right\}^2\frac{2\gamma M^2\tau^2-(\gamma-1)(1+\tau^2)}{2M^2\tau^2}\left(1-\frac{\delta}{\tau}\right)^2\leq\frac{1}{\gamma+1}\frac{M^2-1}{M^4},$$

which may be considered to be negligible compared with unity. Thus, Eq. (4.1.4) may be expressed in a simple form

$$\rho=\frac{\psi_r-\tau^2\psi_x}{r}.\quad(4.1.6)$$

Eq. (4.1.6) has two kinds of error; the one is due to the basic conical flow, $(1/\gamma+1)(M^2-1/M^4)$, and the another is caused by neglecting the terms of order of δ^3/τ. However, the former seems to be over-estimation for a reason that it has been obtained at $\delta/\tau=0$, which implies that no body and, hence, no disturbance exists in the flow field. In such a case, since the second term in right-hand side of Eq. (4.1.5) must be canceled by sum of the remainder terms, so that the actual error may be expected to be much less than $(1/\gamma+1)(M^2-1/M^4)$ for finite value of δ/τ. This circumstance implicitly suggests that the error involved in Eq. (4.1.6) may be of order of δ^3/τ.

By use of Eq. (4.1.6) the fundamental equation for the second-order supersonic axially symmetric small disturbance flow is found to have the form

$$\begin{aligned}&\psi_r^2\psi_{xx}-2\psi_x\psi_r\psi_{xr}+\psi_x^2\psi_{rr}\\&=\frac{\psi_r^{\gamma+1}}{r^{\gamma-1}}\left\{\gamma\omega\left(\psi_{rr}-\frac{1}{r}\psi_r\right)+\omega'\psi_r\right\}\\&\quad+\tau^2\frac{\psi_r^\gamma}{r^{\gamma-1}}\left\{\gamma\omega\psi_x\psi_{xr}+\omega'\psi_r\psi_x^2-\gamma\omega\psi_r\left(\psi_{xr}-\frac{1}{r}\psi_x\right)\right.\\&\qquad\left.-\gamma^2\omega\psi_x\left(\psi_{rr}-\frac{1}{r}\psi_r\right)-\omega'(\gamma+1)\psi_x\psi_r^2\right\},\end{aligned}\quad(4.1.7)$$

where terms of order of δ^3/τ and $\tau^2\delta^2$ have been neglected in the above equation (see Note, p. 49).

In Fig. 9 is presented an example for variation of semi-vertex angle of bodies of revolution with free stream Mach number, in which δ^3/τ and $\tau^2\delta^2$ are used as parameters. In the figure the hatched region bounded by lines having $\delta^3/\tau=\tau^2\delta^2=0.05$ indicates the domain in which Eq. (4.1.7) may be applicable within 5 percents error. A boundary having $\tau\delta=0.05$ is also shown for comparison. Van

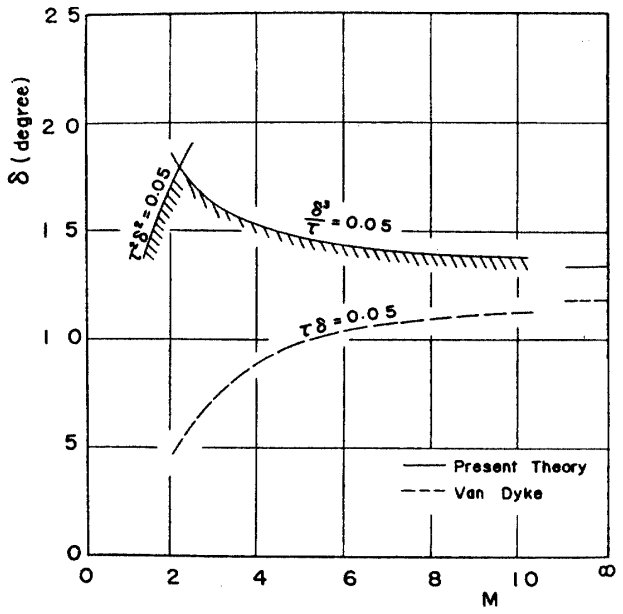

FIGURE 9. Range of applicability of the present theory for axially symmetric flow, Eq. (4.1.7).

Dyke's first-order theory may be applicable in the region under this boundary within 5 percents error. As is seen in the figure, the present theory may be applicable comparatively thick bodies at all supersonic Mach numbers above the transonic.

4.2. *Flow Past Circular-Cones*

As a simple example, consider the supersonic flow past a cone of semi-vertex angle δ. Since the flow field is conical, the stream function and the shock shape can be written in the forms

$$\psi(x, r)=xf(\theta), \qquad \theta=\frac{r}{x}, \tag{4.2.1}$$

$$r_s=S(x)=x. \tag{4.2.2}$$

The shock wave being straight, the flow downstream of the shock wave is irrotational and isentropic, so that the entropy function ω is constant everywhere between shock waves equal to ω_0, which is given by Eq. (3.3.4). It follows that the fundamental equation becomes a non-linear ordinary differential equation

$$f''\left[4f^2-\gamma\omega_0\frac{f'^{\gamma}}{\theta^{\gamma-1}}(f'+\tau^2\{(\gamma+1+\theta)\theta f'-2(\gamma+1)f\})\right]$$

$$=2ff'^2-\gamma\omega_0\frac{f'^{\gamma+1}}{\theta^{\gamma}}[f'+\tau^2\{(\gamma+2+\theta)\theta f'-2(\gamma+1+\theta)f\}]. \tag{4.2.3}$$

and the boundary conditions for $f(\theta)$ at the shock wave is written as

$$\left.\begin{aligned} f(1)&=\frac{1}{2}, \\ f'(1)&=\bar{A}_0. \end{aligned}\right\} \tag{4.2.4}$$

Another boundary condition requires that the stream function vanishes at the cone surface.

$$f(\theta_b)=0\,. \tag{4.2.5}$$

Numerical integration was carried out for several examples step by step inward from the shock wave until f vanishes. However, before discussing the detailed results of the numerical calculations, the validity of Eq. (4.1.6) must be confirmed.

For the conical flow Eq. (4.1.6) can be written as

$$\rho=\frac{f'-\tau^2(2f-\theta f')}{\theta}\,. \tag{4.2.6}$$

On the other hand, Bernoulli's equation for the conical flow has the form

$$\left.\begin{aligned}\tilde{\alpha}\rho^2-\frac{2\gamma}{\gamma-1}\tau^2\omega_0\rho^{\gamma+1}&=\frac{f'^2+\tau^2(2f-\theta f')^2}{\theta^2}\,,\\ \tilde{\alpha}&=1+\frac{2}{(\gamma-1)M^2}\,.\end{aligned}\right\} \tag{4.2.7}$$

Therefore, the confirmation will be made by comparing ρ calculated from Eq. (4.2.6) with that from Eq. (4.2.7), which are shown in Tables 1 to 3. The values

TABLE 1. Reduced density in conical field.

	$M=2$	$\delta=20.77$
	Eq. (4.2.6)	Eq. (4.2.7)
θ	ρ	ρ
1.00	1.348	1.348
0.90	1.458	1.467
08.0	1.528	1.538
0.70	1.589	1.597
0.60	1.644	1.642
0.5031	1.691	1.668

TABLE 2. Reduced density in conical field.

	$M=3$	$\delta=20.57$
	Eq. (4.2.6)	Eq. (4.2.7)
θ	ρ	ρ
1.00	1.831	1.832
0.90	1.967	1.971
0.80	2.061	2.063
0.70	2.154	2.155
0.6605	2.163	2.166

TABLE 3. Reduced density in conical field.

	$M=5$	$\delta=20.40$
	Eq. (4.2.6)	Eq. (4.2.7)
θ	ρ	ρ
1.00	2.820	2.821
0.95	2.937	2.939
0.90	3.025	3.028
0.85	3.090	3.092
0.80	3.132	3.132
0.7910	3.133	3.134

of f and f' used in the computation are those obtained from Eq. (4.2.3). As is seen in the tables, the agreement between Eq. (4.2.6) and Eq. (4.2.7) is found to be quite good. Since the final value of θ in each table indicates cone surface, the error in ρ calculated from Eq. (4.2.6) is within 0.1 percent relative to the one from Eq. (4.2.7) except for the case of Mach number of 2, for which it is at most 2 percents. Comparatively large error for $M=2$, however, is due clearly to the large value of τ ($=0.7536$). For smaller semi-vertex angle than 20° the error will be reduced, thus confirming the validity of Eq. (4.1.6).

In Figs. 10a to 10c are presented the variations of surface pressure coefficient for cone at Mach numbers of 2, 3 and 5, respectively, with semi-vertex angle. In each figure the results obtained from linearized theory, exact conical theory [*10*] and hypersonic small disturbance theory [*8*] are also shown for comparison. As is seen in the figures, the agreement between present theory and the exact conical theory is quite good for semi-vertex angle up to 15°, above which the former predicts pressures that are slightly high in comparison with the latter. However,

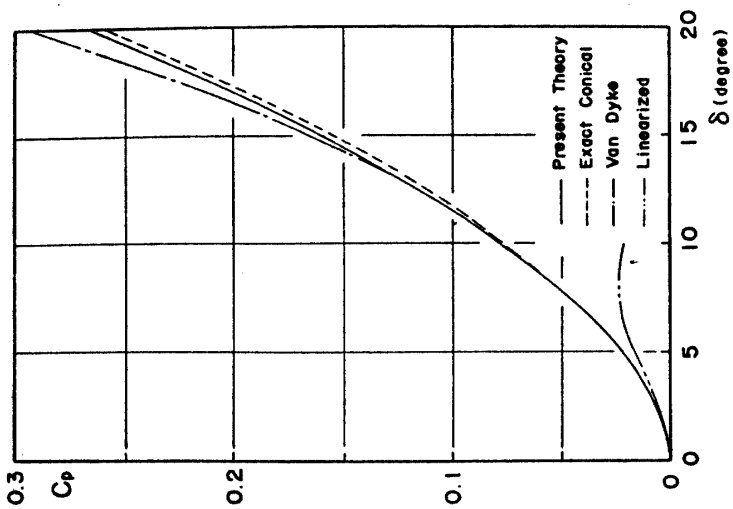

FIGURE 10c. Surface pressure on circular-cone, $M=5$.

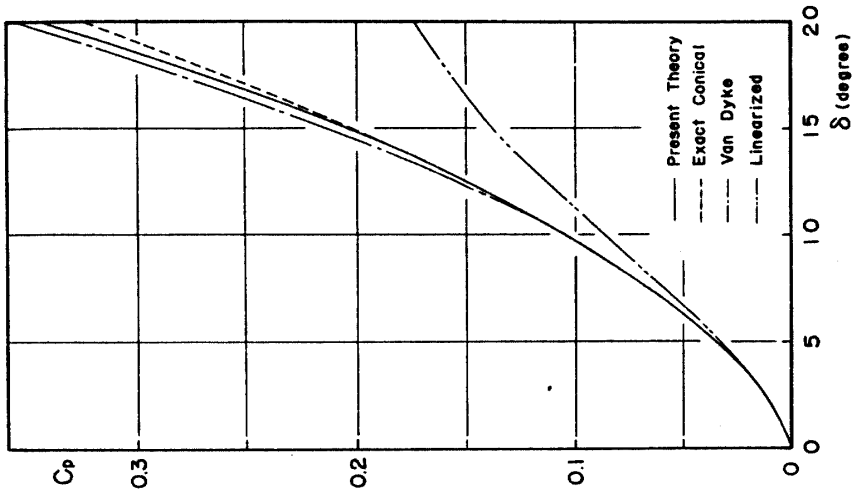

FIGURE 10b. Surface pressure on circular-cone, $M=3$.

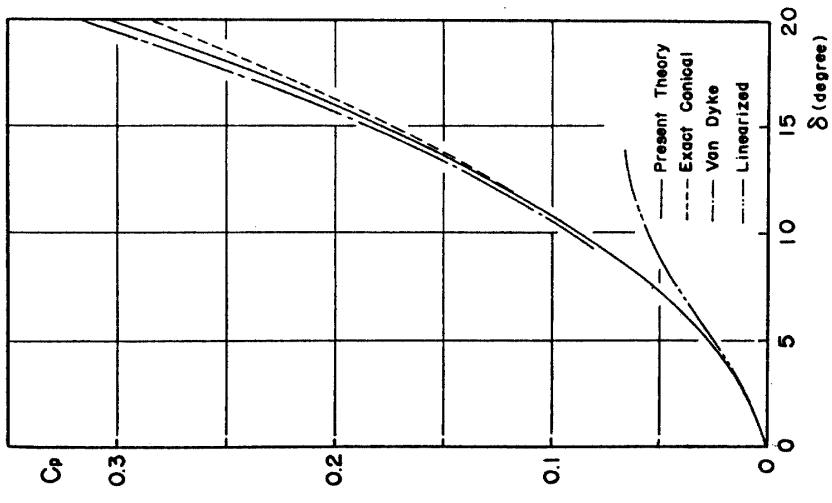

FIGURE 10a. Surface pressure on circular-cone, $M=2$.

the error is only about 5 percents at semi-vertex angle of 20°. It must be remarkable that the linearized theory seems to be useful for semi-vertex angle up to 5°, above which is increasingly inaccurate. This trend grows as Mach number increases. The first-order hypersonic small disturbance theory is found to be less accurate than the present theory.

Figs. 11a to 11c show the variation of shock wave angle for cone with semi-vertex angle in which the results from the exact conical theory and the hypersonic small disturbance theory are also presented for comparison. The agreement between present theory and the exact conical theory is found to be fairly good except for a fact that the present theory gives slightly lower evaluation for the shock wave angle than the exact one. The hypersonic small disturbance theory seems to be less accurate than the present, as is seen in the figures.

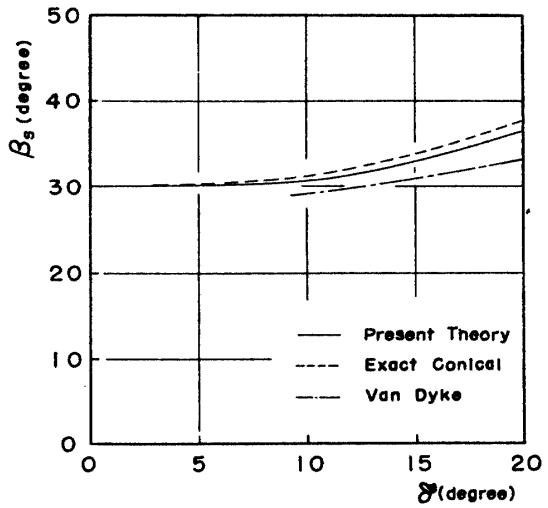

FIGURE 11a. Variation of shock wave angle with semi-vertex angle for circular-cone, $M=2$.

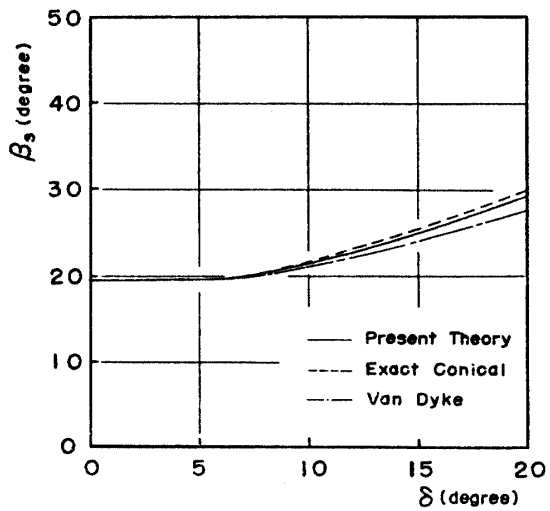

FIGURE 11b. Variation of shock wave angle with semi-vertex angle for circular-cone, $M=3$.

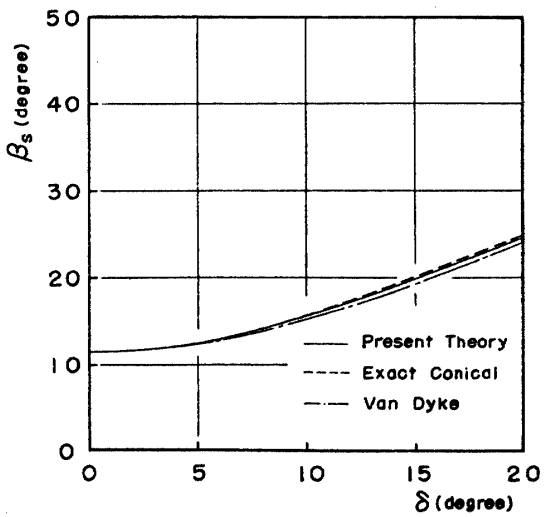

FIGURE 11c. Variation of shock wave angle with semi-vertex angle for circular-cone, $M=5$.

4.3. *Application to Convex Bodies of Revolution*

Consider the supersonic flow past a convex body of revolution with an attached shock wave (see Fig. 1). This problem has already been investigated by Shen and Lin [7] by use of perturbation scheme from full equations, aiming at determination of the initial gradients of the flow properties at the tip of the ogival body of revolution. In clarifying the behaviour of the solution near the surface in their work, however, was misconstrued to indicate a singularity which implied wrongly that the initial pressure gradient at the tip of the ogive is infinite.

On the other hand, the solution given by Van Dyke in his hypersonic small disturbance theory [8] shows no such singularity. According to his argument it seems unlikely that a singularity could have disappeared as a result of making the small disturbance approximation, since this would imply that the approximate model does not retain the essential feature of the full problems.

In the present approach, the flow behind the shock wave is considered to consist of a basic conical flow field upon which is superimposed a perturbation field due to body curvature, as was done by Van Dyke. However, if the stream function is expressed in the same form as Eq. (3.4.2), detailed examination reveals that the similar solutions for the higher power of x become non-analytic near the surface of the basic cone $\theta=\theta_0$, under which the solutions does not exist. This mathematical difficulty together with the fact that the body surface lies under θ_0 for conventional convex body of revolution suggests that the solution for $\psi(x, r)$ cannot be continued beyond the singularity to the body surface. In order to avoid this difficulty, however, it is convenient, as Van Dyke pointed out, to introduce a slightly strained radial coordinate $\tilde{r}$ such that the body surface is given by $\tilde{r}_0=\theta_0 x$.

Let the body surface be given by

$$r_b=\theta_0 x+\frac{1}{2}l\theta_1 x^2+\frac{1}{3}m\theta_2 x^3+\cdots, \tag{4.3.1}$$

and the corresponding shock wave by

$$r_s=x-\frac{1}{2}lx^2-\frac{1}{3}mx^3-\cdots, \tag{4.3.2}$$

then, the simplest choice for $\tilde{r}$ is

$$\tilde{r}=r-\left(\frac{1}{2}l\theta_1 x^2+\frac{1}{3}m\theta_2 x^3+\cdots\right). \tag{4.3.3}$$

Therefore, the conical parameter $\tilde{\theta}$ in the strained coordinates system is expressed as

$$\tilde{\theta}=\frac{\tilde{r}}{x}=\theta-\left(\frac{1}{2}l\theta_1 x+\frac{1}{3}m\theta_2 x^2+\cdots\right). \tag{4.3.4}$$

If the stream function and entropy function are expressed in the forms

$$\psi(x, \tilde{r})=x^2 f(\tilde{\theta})-lx^3\left\{g(\tilde{\theta})-\frac{1}{2}\theta_1 f'(\tilde{\theta})\right\}-mx^4\left\{h(\tilde{\theta})-\frac{1}{3}\theta_2 f'(\tilde{\theta})\right\}$$
$$-l^2x^4\left\{i(\tilde{\theta})+\frac{1}{2}\theta_1 g'(\tilde{\theta})-\frac{1}{8}\theta_1^2 f''(\tilde{\theta})\right\}-\cdots, \tag{4.3.5}$$

$$\omega(\psi)=\omega_0(1-\omega_1 l\sqrt{2\psi}-\bar{\omega}_2 m\psi-\cdots\cdots), \tag{4.3.6}$$

then, the differential equation for each of the similar solutions has, with respect to $\tilde{\theta}$, the same functional form that can be obtained in the unstrained coordinates system, where the stream function is defined by Eq. (3.4.2). Thus, the equation for $f(\tilde{\theta})$ and its boundary conditions are given by Eqs. (4.2.3), (4.2.4) and (4.2.5), respectively, in which $\tilde{\theta}$ and θ_b are replaced by θ and θ_0, respectively.

Equation for g which results in substitution of Eq. (4.3.5) into Eq. (4.1.7) is a linear ordinary differential equation and is written in the form

$$Dg''=A+Bg+Cg', \tag{4.3.7}$$

where

$$\begin{aligned}
A=&-\omega_0\omega_1\frac{f'^{\gamma+1}}{\tilde{\theta}^{\gamma-1}}\left\{\frac{f'^2}{\sqrt{2f}}-\gamma\sqrt{2f}\left(\frac{f'}{\tilde{\theta}}-f''\right)\right\}\\
&-\tau^2\omega_0\omega_1\frac{f'^{\gamma+1}}{\tilde{\theta}^{\gamma-1}}\{2f-(\gamma+1+\tilde{\theta})f'\}\frac{2f-\tilde{\theta}f'}{\sqrt{2f}}\\
&-\tau^2\omega_0\omega_1\frac{f'^{\gamma}}{\tilde{\theta}^{\gamma-1}}\sqrt{2f}\left\{2f-\tilde{\theta}f')(f'-\tilde{\theta}f'')-f'(f'-\tilde{\theta}f''\right.\\
&\left.+\frac{\gamma+1}{\tilde{\theta}}f'(2f-\tilde{\theta}f')-\gamma f''(2f-\tilde{\theta}f')\right\},\\
B=&12ff''-3\tau^2\gamma\omega_0\frac{f'^{\gamma+1}}{\tilde{\theta}^{\gamma-1}}\left\{\frac{\gamma+\tilde{\theta}}{\tilde{\theta}}\left(1-\tilde{\theta}\frac{f''}{f'}\right)+\frac{1}{\tilde{\theta}}\right\},\\
C=&\gamma\omega_0\frac{f'^{\gamma+1}}{\tilde{\theta}^{\gamma-1}}\left\{\frac{\gamma+2}{\tilde{\theta}}-(\gamma+1)\frac{f''}{f'}\right\}-8ff'\\
&-\tau^2\gamma\omega_0\frac{f'^{\gamma-1}}{\tilde{\theta}^{\gamma-1}}\left\{(f'-\tilde{\theta}f'')[(2\gamma f-(\gamma+1)(1+\tilde{\theta})f')]+2f'(2f-\tilde{\theta}f')\right.\\
&\left.-(\gamma+3)f'^2+\frac{(\gamma+1)^2}{\tilde{\theta}}f'(2f-\tilde{\theta}f')-\gamma^2f''(2f-\tilde{\theta}f')+\gamma\tilde{\theta}f'f''\right\},\\
D=&\gamma\omega_0\frac{f'^{\gamma+1}}{\tilde{\theta}^{\gamma-1}}-4f^2-\tau^2\gamma\omega_0\frac{f'^{\gamma}}{\tilde{\theta}^{\gamma-1}}\{(\gamma+\tilde{\theta})(2f-\tilde{\theta}f')-\tilde{\theta}f'\}.
\end{aligned} \tag{4.3.8}$$

Conditions along the shock wave can be obtained from Eqs. (3.4.4a) and (3.4.4b) by replacing $(\psi_r)_s$ by $(\psi_r/r)_s$ and $(-\psi_x)_s$ by $(-\psi_x/r)_s$, respectively. Thus, the boundary conditions for g are written as

$$\left.\begin{aligned}
g(1)&=-\frac{1}{2}\bar{B}_0,\\
g'(1)&=\frac{1}{2}\{f'(1)-f''(1)\}-\bar{A}_1,
\end{aligned}\right\} \tag{4.3.9}$$

where

$$f''(1)=\frac{f'^2(1)-\gamma\omega_0 f'^{\gamma+1}(1)[f'(1)+\tau^2\{(\gamma+3)f'(1)-(\gamma+2)\}]}{1-\gamma\omega_0 f'^{\gamma}(1)[f'(1)+\tau^2\{(\gamma+2)f'(1)-(\gamma+1)\}]}. \tag{4.3.10}$$

Since the function f associated with the basic conical flow vanishes at the surface $\tilde{\theta}=\theta_0$, the coefficient A in the differential equation for g becomes infinite

at $\tilde{\theta}=\theta_0$. This indicates that the function g becomes non-analytic near the surface. On the other hand, the fact that f is analytic near the surface leads to a series expansion of f as

$$f(\tilde{\theta})=(\tilde{\theta}-\theta_0)f'(\theta_0)+O[(\tilde{\theta}-\theta_0)^2]\,. \tag{4.3.11}$$

It follows that near the surface the coefficients of the differential equation for g behave like

$$\begin{aligned} &A\sim -A_0(\tilde{\theta}-\theta_0)^{-\frac{1}{2}}\,,\\ &B\sim B_0\,,\\ &C\sim C_0\,,\\ &D\sim D_0\,, \end{aligned} \tag{4.3.12}$$

where

$$\begin{aligned} A_0&=\frac{1}{\sqrt{2}}\omega_0\omega_1\frac{f_0'^{\gamma+\frac{1}{2}}}{\theta_0^{\gamma-1}}\{1+\tau^2\theta_0(\gamma+1+\theta_0)\}\,,\\ B_0&=-3\tau^2\gamma\omega_0\frac{f_0'^{\gamma+1}}{\theta_0^{\gamma-1}}\left\{\frac{\gamma+\theta_0}{\theta_0}\left(1-\theta_0\frac{f_0''}{f_0'}\right)+\frac{1}{\theta_0}\right\},\\ C_0&=\gamma\omega_0\frac{f_0'^{\gamma+1}}{\theta_0^{\gamma-1}}\left\{\frac{\gamma+2}{\theta_0}-(\gamma+1)\frac{f_0''}{f_0'}\right\}+\tau^2\gamma\omega_0\frac{f_0'^{\gamma+1}}{\theta_0^{\gamma-1}}\left\{(\gamma+1)(1+\theta_0)\left(1-\theta_0\frac{f_0''}{f_0'}\right)\right.\\ &\qquad\left.+(\gamma^2+3\gamma+4)+2\theta_0-\gamma(\gamma+1)\theta_0\frac{f_0''}{f_0'}\right\},\\ D_0&=\gamma\omega_0\frac{f_0'^{\gamma+1}}{\theta_0^{\gamma-1}}\{1+\tau^2\theta_0(\gamma+1+\theta_0)\}\,. \end{aligned} \tag{4.3.13}$$

and where subscript o denotes the condition at $\tilde{\theta}=\theta_0$ and

$$\frac{f_0''}{f_0'}=\frac{1}{\theta_0}\,\frac{1+\tau^2\theta_0(\gamma+2+\theta_0)}{1+\tau^2\theta_0(\gamma+1+\theta_0)}\,. \tag{4.3.14}$$

Although the point $\tilde{\theta}=\theta_0$ is a singular point of Eq. (4.3.7), it is an ordinary point of the homogeneous equation by deleting A. Therefore, the general solution of the homogeneous equation is analytic, while the particular solution of the non-homogeneous equation has $^3/_2$-power branch point at $\tilde{\theta}=\theta_0$. This arises from the fact that the pencil of fluid striking the tip of the ogive is spread thin over the entire surface and the linear entropy gradient at the tip due to a curved shock wave is intensified to a square-root gradient normal to the surface elsewhere.

The two unknown constants involved in the general solution of the homogeneous equation can be determined as the values of g and its first derivative at $\tilde{\theta}=\theta_0$. Thus, the full solution of Eq. (4.3.7) can be obtained near the surface as

$$\begin{aligned} g(\tilde{\theta})=&-\frac{4}{3}\,\frac{A_0}{D_0}(\tilde{\theta}-\theta_0)^{\frac{3}{2}}\left\{1+\frac{2}{5}\,\frac{C_0}{D_0}\varepsilon+\frac{4}{35}\left(\frac{C_0^2}{D_0^2}+\frac{B_0}{D_0}\right)\varepsilon^2+\cdots\right\}\\ &+g(\theta_0)\left\{1+\frac{1}{2}\,\frac{B_0}{D_0}\varepsilon^2+\frac{1}{6}\,\frac{B_0}{D_0}\,\frac{C_0}{D_0}\varepsilon^3+\cdots\right\}\\ &+g'(\theta_0)\varepsilon\left\{1+\frac{1}{2}\,\frac{C_0}{D_0}\varepsilon+\frac{1}{6}\left(\frac{C_0^2}{D_0^2}+\frac{B_0}{D_0}\right)\varepsilon^2+\cdots\right\}, \end{aligned} \tag{4.3.15}$$

where

$$\varepsilon=\tilde{\theta}-\theta_0 .$$

The integration of Eq. (4.3.7) is carried out numerically step by step inward starting from the known values at $\tilde{\theta}=1$ and using the same intervals for $\tilde{\theta}$. The step by step solution is then joined at the two points in the very vicinity of $\tilde{\theta}=\theta_0$ with the series expansion about the singular point given by Eq. (4.3.15). Thus, $g(\theta_0)$ and $g'(\theta_0)$ are determined and the solution for g is obtained.

Differential equations for h and i are expressed, respectively, as

$$Dh''=E+Fh+Gh' , \tag{4.3.16}$$

$$Di''=I+Fi+Gi' , \tag{4.3.17}$$

where D is given in Eq. (4.3.13), and where

$$F=4(f'^2+4ff'')-4\tau^2\gamma\omega_0\frac{f'^{\gamma+1}}{\tilde{\theta}^{\gamma-1}}\left\{\frac{\gamma+\tilde{\theta}}{\tilde{\theta}}\left(1-\tilde{\theta}\frac{f''}{f'}\right)+\frac{1}{\tilde{\theta}}\right\},$$

$$G=\gamma\omega_0\frac{f'^{\gamma+1}}{\tilde{\theta}^{\gamma-1}}\left\{\frac{\gamma+2}{\tilde{\theta}}-(\gamma+1)\frac{f''}{f'}\right\}-12ff'-\tau^2\gamma\omega_0\frac{f'^{\gamma-1}}{\tilde{\theta}^{\gamma-1}}\times$$
$$\left[\{2\gamma f-(\gamma+1)(1+\tilde{\theta})f'\}(f'-\tilde{\theta}f'')+3f'(2f-\tilde{\theta}f')-(\gamma+4)f'^2\right.$$
$$\left.+\frac{(\gamma+1)^2}{\tilde{\theta}}f'(2f-\tilde{\theta}f')-\gamma^2f''(2f-\tilde{\theta}f')+\gamma\tilde{\theta}f'f''\right],$$

$$E=-2\omega_0\omega_1\frac{f'^{\gamma+1}}{\tilde{\theta}^{\gamma-1}}\left\{\gamma f\left(f''-\frac{f'}{\tilde{\theta}}\right)+f'^2\right\}$$
$$-2\tau^2\gamma\omega_0\omega_1\frac{ff'^{\gamma}}{\tilde{\theta}^{\gamma-1}}\left\{(2f-\tilde{\theta}f')(f'-\tilde{\theta}f'')-f'(f'-\tilde{\theta}f'')\right.$$
$$\left.-\gamma f''(2f-\tilde{\theta}f')+\frac{\gamma+1}{\tilde{\theta}}f'(2f-\tilde{\theta}f')\right\}$$
$$-2\tau^2\omega_0\omega_1\frac{f'^{\gamma+1}}{\tilde{\theta}^{\gamma-1}}\left\{\gamma f\left(f''-\frac{f'}{\tilde{\theta}}\right)+f'^2\right\},$$

$$I=I_1+I_2 ,$$

$$I_1=\omega_0(2\alpha-\omega_1)\frac{f'^{\gamma+1}}{\tilde{\theta}^{\gamma-1}}\left\{\gamma f\left(f''-\frac{f'}{\tilde{\theta}}\right)+f'^2\right\}$$
$$+\tau^2\gamma\omega_0(2\alpha-\omega_1)\frac{ff'^{\gamma}}{\tilde{\theta}^{\gamma-1}}\left\{(2f-\tilde{\theta}'f)(f'-\tilde{\theta}f'')-f'(f'-\tilde{\theta}f'')\right.$$
$$\left.-\gamma f''(2f-\tilde{\theta}f')+\frac{\gamma+1}{\tilde{\theta}}f'(2f-\tilde{\theta}f')\right\}$$
$$+\tau^2\omega_0(2\alpha-\omega_1)\frac{f'^{\gamma+1}}{\tilde{\theta}^{\gamma-1}}(2f-\tilde{\theta}f')\{2f-(\gamma+1+\tilde{\theta})f'\},$$

$$I_2=3(2fg'^2+2f'gg'-4fgg''-3f''g^2)$$
$$+\gamma(\gamma+1)\omega_0\frac{f'^{\gamma}}{\tilde{\theta}^{\gamma-1}}g'^2\left(\frac{1}{2}\gamma\frac{f''}{f'}+\frac{g''}{g'}-\frac{\gamma+2}{2\tilde{\theta}}\right)$$

(continued to the next page)

$$
\begin{aligned}
&-\omega_0\omega_1\frac{f'^{\gamma+1}}{\tilde{\theta}^{\gamma-1}}\frac{g}{(2f)^{\frac{3}{2}}}\{f'^2+\tau^2(2f-\tilde{\theta}f')[2f-(\gamma+1+\tilde{\theta})f']\}\\
&+\omega_0\omega_1\frac{f'^{\gamma+1}}{\tilde{\theta}^{\gamma-1}}\frac{g}{\sqrt{2f}}\left\{\gamma\left(f''-\frac{f'}{\tilde{\theta}}\right)+(\gamma+3)f'\frac{g'}{g}\right\}\\
&+\gamma\omega_0\omega_1\frac{f'^{\gamma+1}}{\tilde{\theta}^{\gamma-1}}g'\sqrt{2f}\left\{(\gamma+1)\frac{f''}{f'}+\frac{g''}{g'}-\frac{\gamma+2}{\tilde{\theta}}\right\}\\
&+\tau^2\gamma\omega_0\frac{f'^{\gamma-2}}{\tilde{\theta}^{\gamma-1}}\Big[\frac{1}{2}\gamma g'^2\left\{(\gamma-1)(2f-\tilde{\theta}f')(f'-\tilde{\theta}f'')-(\gamma+1)f'(f'-\tilde{\theta}f'')\right.\\
&\quad\left.-\gamma(\gamma-1)f''(2f-\tilde{\theta}f')+\frac{(\gamma+1)^2}{\tilde{\theta}}f'(2f-\tilde{\theta}f')\right\}+f'g'(3g-\tilde{\theta}g')\left\{\gamma(f'-\tilde{\theta}f'')\right.\\
&\quad\left.-\gamma^2f''+\frac{(\gamma+1)^2}{\tilde{\theta}}f'\right\}+f'g'(2g'-\tilde{\theta}g'')\{\gamma(2f-\tilde{\theta}f')-(\gamma+1)f'\}\\
&\quad+f'^2(3g-\tilde{\theta}g')(2g'-\tilde{\theta}g'')-\gamma^2f'g'g''(2f-\tilde{\theta}f')-\gamma f'^2g''(3g-\tilde{\theta}g')\Big]\\
&+\tau^2\gamma\omega_0\omega_1\frac{f'^{\gamma}}{\tilde{\theta}^{\gamma-1}}\frac{g}{\sqrt{2f}}\left\{(2f-\tilde{\theta}f')(f'-\tilde{\theta}f'')-f'(f'-\tilde{\theta}f'')\right.\\
&\qquad\left.+\frac{\gamma+1}{\tilde{\theta}}f'(2f-\tilde{\theta}f')-\gamma f''(2f-\tilde{\theta}f')\right\}\\
&+\tau^2\omega_0\omega_1\frac{f'^{\gamma}}{\tilde{\theta}^{\gamma-1}}\frac{1}{\sqrt{2f}}\{(\gamma+1)(2f-\tilde{\theta}f')[2f-(\gamma+2+\tilde{\theta})f']g'\\
&\qquad+f'(3g-\tilde{\theta}g')[4f-(\gamma+1+2\tilde{\theta})f']\}\\
&+\tau^2\gamma\omega_0\omega_1\frac{f'^{\gamma-1}}{\tilde{\theta}^{\gamma-1}}\sqrt{2f}\Big[g'\left\{\gamma(2f-\tilde{\theta}f')(f'-\theta f'')-\gamma^2f''(2f-\tilde{\theta}f')\right.\\
&\qquad\left.-(\gamma+1)f'(f'-\tilde{\theta}f'')+\frac{(\gamma+1)^2}{\tilde{\theta}}f'(2f-\tilde{\theta}f')\right\}\\
&\qquad+f'(3g-\tilde{\theta}g')\left\{\frac{\gamma+\tilde{\theta}}{\tilde{\theta}}(f'-\tilde{\theta}f'')+\frac{f'}{\tilde{\theta}}\right\}\\
&\qquad+f'\{2f-(1+\tilde{\theta})f'\}(2g'-\tilde{\theta}g'')-\gamma f'(2f-\tilde{\theta}f')g''\Big]. \qquad (4.3.18)
\end{aligned}
$$

The boundary conditions for h and i are given, respectively, as

$$
\left.\begin{aligned}
h(1)&=-\frac{1}{3}\bar{B}_0,\\
h'(1)&=\frac{1}{3}\{f'(1)-f''(1)\}-\bar{A}_0,
\end{aligned}\right\} \qquad (4.3.19)
$$

$$
\left.\begin{aligned}
i(1)&=\frac{1}{4}\Big[\bar{B}_2-\bar{A}_2+\frac{1}{4}\{f'(1)-f''(1)+2g'(1)\}\Big],\\
i'(1)&=\frac{1}{2}\Big[\frac{1}{4}f'''(1)-\frac{1}{2}f''(1)+\frac{1}{2}f'(1)+g''(1)-g'(1)\Big],
\end{aligned}\right\} \qquad (4.3.20)
$$

where $\bar{B}_0$, $\bar{A}_1$, $\bar{A}_2$ and $\bar{B}_2$ are given by Eq. (3.4.4c), and

$$f'''(1)=\frac{1}{1-\gamma\omega_0 f''^{\gamma}(1)[f'(1)+\tau^2\{(\gamma+2)f'(1)-(\gamma+1)\}]}\times$$
$$[\{f''^2(1)-f''(1)\}\{\gamma+2f'(1)\}+\gamma(\gamma+1)\omega_0 f''^{\gamma}(1)f''(1)\{f''(1)-f'(1)\}$$
$$+\tau^2\gamma\omega_0 f''^{\gamma-1}(1)\{\gamma(\gamma+2)f'(1)f''(1)+(\gamma+1)(\gamma+2)f'(1)f''^2(1)$$
$$+f'^2(1)+\gamma f'^3(1)-\gamma(\gamma+1)f''^2(1)-(\gamma^2+5\gamma+3)f'^2(1)f''(1)\}]\,. \tag{4.3.21}$$

It is clear that the function h is analytic everywhere while the function i is non-analytic near the point $\tilde{\theta}=\theta_0$. The same mathematical procedure as was made for $g(\tilde{\theta})$ can be, therefore, applied to clarify the behaveour of i near the singular point, indicating that the particular solution of the nonhomogeneous equation for i has $^1/_2$-power branch point at $\tilde{\theta}=\theta_0$. However, it seems to be convenient to represent the full solution of i near the singular point in the form of not $i(\tilde{\theta})$ itself but the combination $i(\tilde{\theta})+g'(\tilde{\theta})(g_0/f_0')$. Hence, the series employed can be obtained as

$$\begin{aligned} i(\tilde{\theta})+g'(\tilde{\theta})\frac{g_0}{f_0'}=&-\frac{\sqrt{2}\,\omega_1}{3\gamma}f_0'^{\frac{1}{2}}g_0(\tilde{\theta}-\theta_0)^{\frac{3}{2}}\{P_0+2P_1\varepsilon+\cdots\cdot\}\\ &+i(\theta_0)\left\{1+\frac{1}{2}\bar{\lambda}\varepsilon^2+\frac{1}{6}\bar{\lambda}\bar{\mu}\varepsilon^3+\cdots\cdot\right\}\\ &+K(\tilde{\theta}-\theta_0)\left\{1+\frac{1}{2}\bar{\mu}\varepsilon+\frac{1}{6}(\bar{\lambda}+\bar{\mu}^2)\varepsilon^2+\cdots\cdot\right\}\\ &+\frac{1}{2}\bar{\nu}\bar{\lambda}\varepsilon^2\left\{1+\frac{1}{3}\bar{\mu}\varepsilon+\frac{1}{12}(\bar{\lambda}+\bar{\mu}^2)\varepsilon^2+\cdots\cdot\right\}\\ &+\frac{g_0^2}{f_0'}\lambda\varepsilon\left\{1+\frac{1}{2}\mu\varepsilon+\frac{1}{6}(\lambda+\mu^2)\varepsilon^2+\cdots\cdot\right\}\\ &+\frac{g_0g_0'}{f_0'}\left\{1+\mu\varepsilon+\frac{1}{2}(\lambda+\mu^2)\varepsilon^2+\cdots\cdot\right\}, \end{aligned} \tag{4.3.22}$$

where

$$\left.\begin{aligned} &\lambda=\frac{B_0}{D_0}\,,\qquad \mu=\frac{C_0}{D_0}\,,\\ &\bar{\lambda}=\frac{F_0}{D_0}\,,\qquad \bar{\mu}=\frac{G_0}{D_0}\,,\qquad \bar{\nu}=\frac{\tilde{I}_2}{F_0}\,,\\ &P_0=\frac{\tilde{I}_1}{\tilde{I}_0}-2(\bar{\mu}-\mu)\,,\\ &P_1=\frac{1}{5}\left(\frac{\tilde{I}_1}{\tilde{I}_0}\bar{\mu}-2\bar{\mu}^2-2\bar{\lambda}\right)+\frac{2}{5}(\lambda+\mu^2)\,, \end{aligned}\right\} \tag{4.3.23}$$

and where

$$F_0=4f_0'^2-4\tau^2\gamma\omega_0\frac{f_0'^{\gamma+1}}{\theta_0^{\gamma-1}}\left\{\frac{\gamma+\theta_0}{\theta_0}\left(1-\theta_0\frac{f_0''}{f_0'}\right)+\frac{1}{\theta_0}\right\},$$

$$G_0=\gamma\omega_0\frac{f_0'^{\gamma+1}}{\theta_0^{\gamma-1}}\left\{\frac{\gamma+2}{\theta_0}-(\gamma+1)\frac{f_0''}{f_0'}\right\}+\tau^2\gamma\omega_0\frac{f_0'^{\gamma+1}}{\theta_0^{\gamma-1}}\left\{(\gamma+1)(1+\theta_0)\left(1-\theta_0\frac{f_0''}{f_0'}\right)\right.$$
$$\left.+3\theta_0+(\gamma^2+3\gamma+5)-\gamma(\gamma+1)\frac{f_0''}{f_0'}\right\},$$

$$\tilde{I}_0=-\omega_0\omega_1\frac{f_0'^{\gamma+\frac{3}{2}}}{\theta_0^{\gamma-1}}\frac{g_0}{2\sqrt{2}}\{1+\tau^2\theta_0(\gamma+1+\theta_0)\},$$

$$\tilde{I}_1=\omega_0\omega_1\frac{f_0'^{\gamma+\frac{3}{2}}}{\theta_0^{\gamma-1}}\frac{g_0}{\sqrt{2}}\left\{\gamma\left(\frac{f_0''}{f_0'}-\frac{1}{\theta_0}\right)+2\frac{g_0'}{g_0}\right\}+\tau^2\omega_0\omega_1\frac{f_0'^{\gamma+\frac{3}{2}}}{\theta_0^{\gamma-1}}\frac{g_0}{\sqrt{2}}\times$$
$$\left\{\gamma(\gamma+1+\theta_0)\theta_0\frac{f_0''}{f_0'}+2(\gamma+1+\theta_0)\theta_0\frac{g_0'}{g_0}-(\gamma^2+2\gamma+3+\gamma\theta_0+3\theta_0)\right\},$$

$$\tilde{I}_2=-\omega_0\omega_1\frac{f_0'^{\gamma+3}}{\theta_0^{\gamma-1}}\{1+\tau^2\theta_0(\gamma+1+\theta_0)\}+3g_0(2f_0'g_0'-3f_0''g_0)$$
$$+\omega_0(2\alpha-\omega_1)\frac{f_0'^{\gamma+3}}{\theta_0^{\gamma-1}}\{1+\tau^2\theta_0(\gamma+1+\theta_0)\}+\frac{\gamma(\gamma+1)}{2}\omega_0\frac{f_0'^{\gamma}}{\theta_0^{\gamma-1}}g_0'^2\left(\gamma\frac{f_0''}{f_0'}-\frac{\gamma+2}{\theta_0}\right)$$
$$+\tau^2\gamma\omega_0\frac{f_0'^{\gamma}}{\theta_0^{\gamma-1}}\left[\frac{1}{2}\gamma g_0'^2\left\{[\gamma^2+1+(\gamma-1)\theta_0]\theta_0\frac{f_0''}{f_0'}-[(\gamma-1)\theta_0+(\gamma+1)(\gamma+2)]\right\}\right.$$
$$+g_0'(3g_0-\theta_0g_0')\left\{\gamma\left(1-\theta_0\frac{f_0''}{f_0'}\right)-\gamma^2\frac{f_0''}{f_0'}+\frac{(\gamma+1)^2}{\theta_0}\right\}$$
$$\left.+6g_0g_0'-2(\gamma+1)(1+\theta_0)g_0'^2\right]. \tag{4.3.24}$$

The unknown constant K in Eq. (4.3.22) can be obtained from the equation

$$i_0'+g_0''\frac{g_0}{f_0'}=K+\frac{g_0}{f_0'}(\lambda g_0+\mu g_0'). \tag{4.3.25}$$

The differential equations for h and i are also integrated numerically in the same manner as outlined previously. Since $h(\tilde{\theta})$ is regular near the surface of the body, it is readily integrated with ample accuracy. On the other hand, the accuracy of the solution for $i(\tilde{\theta})$ suffers from the facts that it depends upon the accuracy of the preceding solution for $g(\tilde{\theta})$, that one coefficient in the differential equation is singular. Moreover, one coefficient in the differential equation for $i(\tilde{\theta})$ itself indicates a strong singularity at the body surface. Consequently, although results derived from f and g are reliable, those derived from i are probably not so reliable.

Now that the stream function is determined, the body shape can be obtained from the condition that ψ must vanish along the body surface, $\tilde{\theta}=\theta_0$.

$$\psi(x,\theta_0)=0. \tag{4.3.26}$$

By use of Eqs. (4.3.5) and (4.3.26) the radius of the body is expressed as

$$r_b=\theta_0x+\frac{g_0}{f_0'}lx^2+\left\{m\frac{h_0}{f_0'}+l^2\left(\frac{i_0}{f_0'}+\frac{g_0g_0'}{f_0'^2}-\frac{1}{2}\frac{g_0^2}{f_0'^3}f_0''\right)\right\}x^3+\cdots, \tag{4.3.27}$$

where subscript o indicates the value at $\tilde{\theta}=\theta_0$. The unknown constants, l, m, in the above equation are determined by the given body shape.

4.4. *Application to Paraboloid-Arc Bodies of Revolution*

As an example, consider the supersonic flow past paraboloid-arc bodies of revolution, which is given by the equation

$$r_b=\frac{2\tau_0}{\tau}x(1-x), \tag{4.4.1}$$

where τ_0 denotes the ratio of maximum diameter to body length. Therefore, $1/\tau_0$ is the fineness ratio of the body. By comparing Eq. (4.4.1) with Eq. (4.3.27) it is found that

$$\theta_0=\frac{2\tau_0}{\tau}, \tag{4.4.2}$$

$$l=-\theta_0\frac{f_0'}{g_0}=-\frac{2\tau_0}{\tau}\frac{f_0'}{g_0}, \tag{4.4.3}$$

$$m=-\frac{l^2}{h_0}\left\{i_0+g_0'\frac{g_0}{f_0'}-\frac{1}{2}\left(\frac{g_0}{f_0'}\right)^2 f_0''\right\}. \tag{4.4.4}$$

The initial ratio of shock to body curvature and the initial slope of surface pressure coefficient are given, respectively, in the accuracy of the present approximation as

$$\frac{K_s}{K_b}=-\frac{f_0'}{2g_0}, \tag{4.4.5}$$

$$\left(\frac{1}{K_b}\frac{dC_p}{dx}\right)_{x=0}=-\frac{\gamma\omega_0}{2\tau_0}\tau^2\left(\rho_b^{\gamma-1}\frac{d\rho_b}{dx}\right)_{x=0}, \tag{4.4.6}$$

where

$$\rho_b(0)=\frac{(1+\tau^2\theta_0)f_0'}{\theta_0}, \tag{4.4.7a}$$

$$\left(\frac{d\rho_b}{dx}\right)_{x=0}=-\frac{1}{\theta_0}\left[\left(f_0''-\frac{f_0'g_0'}{g_0}-\tau^2\left\{f_0'-\theta_0 f_0''-\frac{f_0'}{g_0}(3g_0-\theta_0 g_0')\right\}\right)\theta_0-(1+\tau^2\theta_0)f_0'\right]. \tag{4.4.7b}$$

In Figs. 12a to 12c is presented the variation of initial ratio of shock wave to body curvature with semi-vertex angle for Mach numbers of 2, 3 and 5, respectively. Results obtaided by Shen and Lin [7] and by Van Dyke [8] are also shown in each figure for comparison. By use of perturbation scheme from initial Taylor-Maccoll [11] conical solution Shen and Lin gave a figure indicating the initial ratio of body to shock wave curvature, for which the numerical computations were carried out for semi-vertex angles of 10°, 20° and 30°, respectively. Therefore, Shen and Lin's data plotted in the present figures by use of round signs were obtained from their faired curves.

The figures show that the present results agree well with those obtained by Shen and Lin. The hypersonic small disturbance theory seems to have less agreement with present theory and Shen and Lin's results. This trend is quite the same as has been already found in the case of plane flow.

Figs. 13a to 13c show the variation of the initial slope of surface pressure coe-

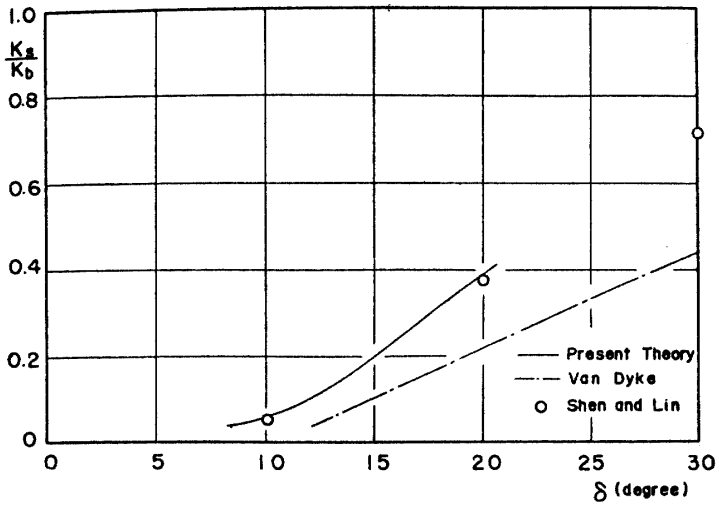

FIGURE 12a. Initial ratio of shock to body curvature for axially symmetric body, $M=2$.

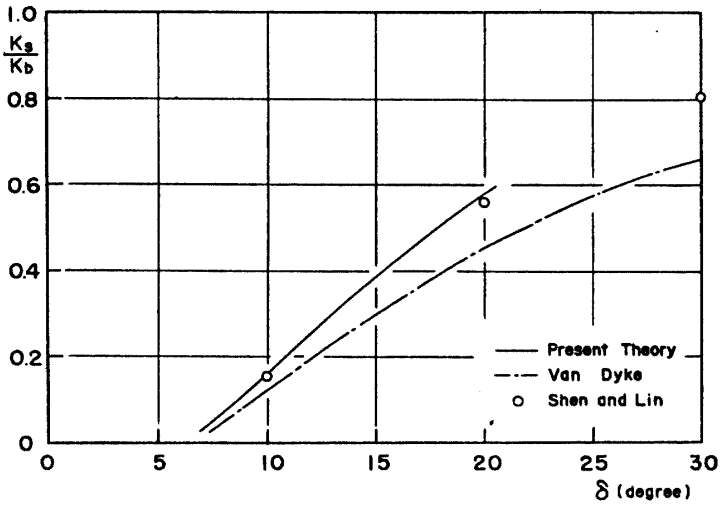

FIGURE 12b. Initial ratio of shock to body curvature for axially symmetric body, $M=3$.

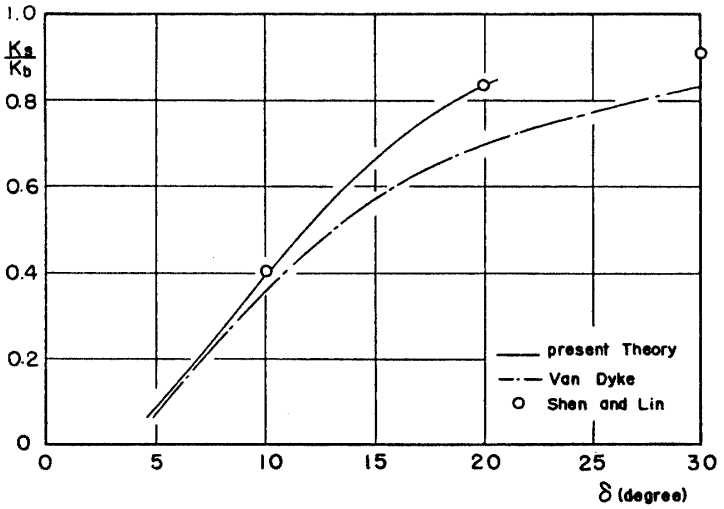

FIGURE 12c. Initial ratio of shock to body curvature for axially symmetric body, $M=5$.

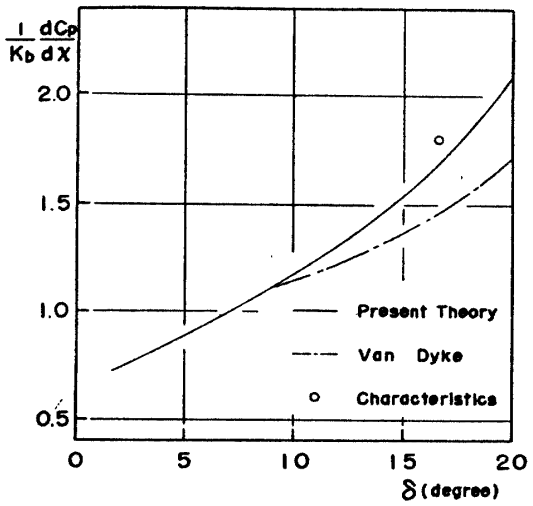

FIGURE 13a. Initial pressure gradient on axially symmetric body, $M=2$.

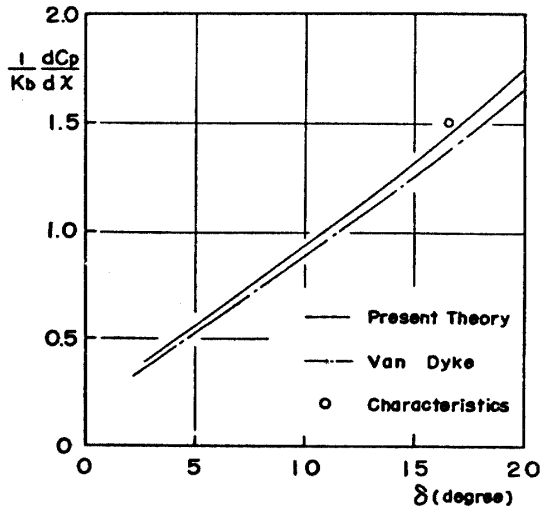

FIGURE 13b. Initial pressure gradeint on axially symmetric body, $M=3$.

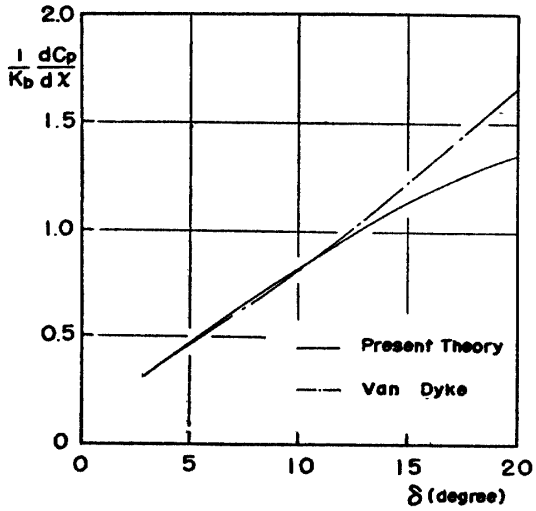

FIGURE 13c. Initial pressure gradient on axially symmetric body, $M=5$.

fficient with semi-vertex angle for Mach numbers of 2, 3 and 5, respectively. The result from hypersonic small disturbance theory is also presented in each figure for comparison. Since there could not be found out any other datum to be compared, numerical computations were carried out for a paraboloid-arc half-body of revolution with $\tau_0=0.1494$ and for Mach numbers of 2 and 3 by use of the method of characteaistics, and the results are plotted in Figs. 13a and 13b, respectively, by the use of round sign.

As is seen in the figures, the present theory is found to have better agreement with the method of characteristics than the hypersonic small disturbance theory. Futhermore, at the tip of the body the present theory does not indicate such a logarithmic singularity as was mentioned by Shen and Lind. Thus, the initial gradient of surface pressure is proved to be always finite for the axially symmetric pointed bodies, as has been already mentioned by Van Dyke [8].

In Figs. 14 and 15 is presented the surface pressure distribution for paraboloid-

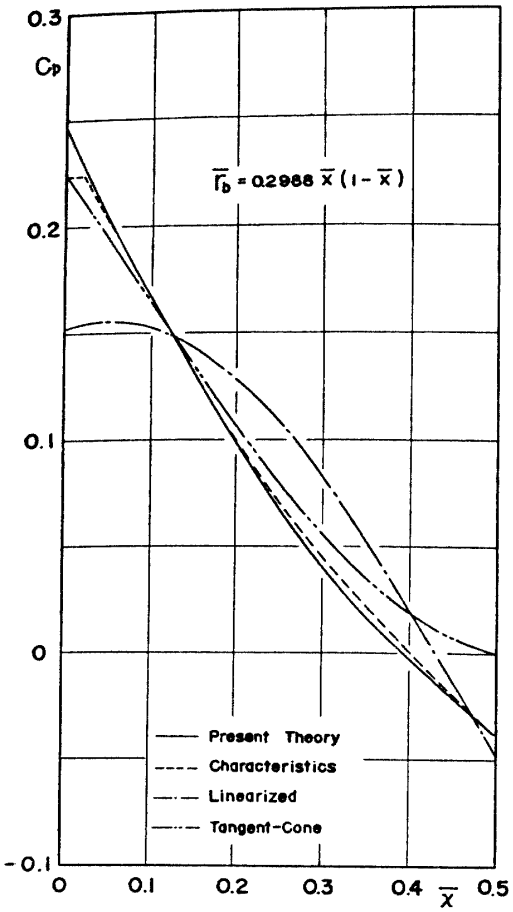

FIGURE 14. Surface pressure distribution on paraboloid-arc half-body of revolution, $M=2$, $\tau_0=0.1494$.

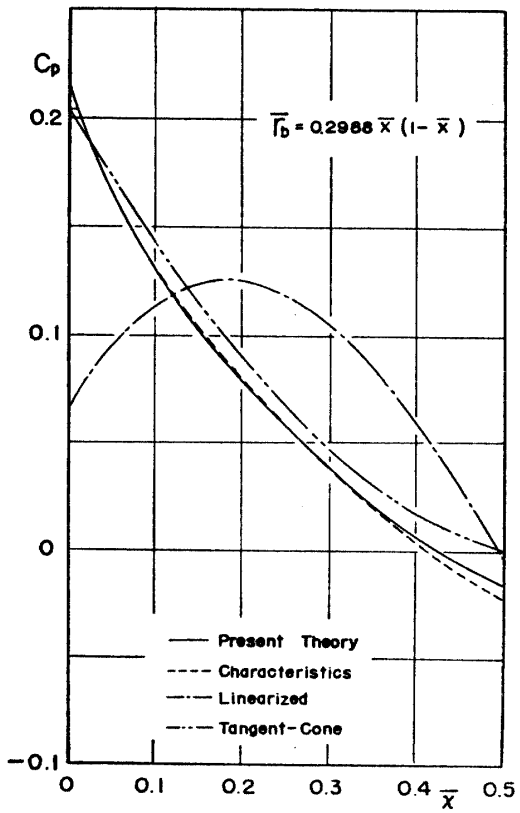

FIGURE 15. Surface pressure distribution on paraboloid-arc half-body of revolution, $M=3$, $\tau_0=0.1494$.

arc half-body of revolution with $\tau_0=0.1494$ and for Mach numbers of 2 and 3, respectively. The results obtained from the method of characteristics, linearized theory and tangent-cone approximation are also shown in each figure for comparison. The agreement between present theory and the method of characteristics is quite good. The tangent-cone approximation seems to be fairly accurate in downstream vicinity of the tip, but it fails as the surface gradient tends to vanish. On the other hand, the linearized theory does not seem to predict the essential feature of the flow. This is clearly due to the inapplicability of the the linearized theory to such a thick body.

5. EXPERIMENT

5.1. *Introductory Remark*

An analytical approach has been developed in previous sections for the second-order plane and axially symmetric flows at supersonic speeds, yielding that the present approach is in good agreement with the method of characteristics. From the practical point of view, however, the shock-expansion method seems to be more accurate and convenient than the present approach in estimating the surface

pressure on the given bodies in plane supersonic flow.

Contrary to the plane problems, in evaluation of the surface pressure on axially symmetric bodies, the linearized theory seems to be the most practical method convenient to use, although it has already been found to be inaccurate for comparatively thick bodies. On the other hand, although the method of characteristics may be exact, the characteristics net-work seems to be very much laborious. In this sense, the present approach for axially symmetric flow may be of great value as a useful approximate method, which has been found to be in good agreement with the method of characteristics.

Experimental confirmation of the present approach is of another interest. Examination of the existing studies reveals that there does not seem to exist much previous works on comparatively thick bodies of revolution with longitudinally curved surface at supersonic speeds, while there are much data for the plane flow. In practice, however, the nose of supersonic projectiles such as missiles and rockets seems to have fairly small fineness ratio, for which the linearized theory is inaccurate. Therefore, it may be worth doing an experimental investigation to present some data on the axially symmetric flows.

The purpose of the present experiment is to confirm the validity of the present theory and to give some experimental data on a paraboloid-arc half-body of revolution with fairly small fineness ratio at supersonic speeds.

5.2. *Wind Tunnel*

The experiment was carried out by use of two wind tunnels. The one is an intermittent blow-down type ordinary supersonic wind tunnel with 40 cm × 40 cm square cross section at the test part. Air reservoir is a steel sphere of 524 m^3 in which dry air is compressed at 15 kg/cm^2 at maximum. Stagnation pressure measured in the settling chamber can be fixed at an arbitrarily given value during the test by use of automatical control system. The error in fixing the stagnation pressure was measured to be within one percent. During the test of about 120 sec. the stagnation temperature was found to be almost constant at the atmospheric value. After that time it decreases gradually due to adiabatic expansion of the air in the reservoir tank. The air used for testing blows into atmosphere through a subsonic diffusor and a silencer.

There are three nozzles designed for fixed Mach numbers of 2, 3 and 4, respectively, so that change in Mach number of the wind tunnel must be made by exchanging the nozzle block. The test chamber can be observed through two glass windows mounted just oppositely on both side-walls of the nozzle block. A photograph of this wind tunnel is shown in Fig. 16.

The another is an intermittent blow-down type hypersonic wind tunnel with an ejector downstream of the test chamber. The air stored in a tank of 4 m^3 and at 120 kg/cm^2 is led through an automatically regulating valve to a constant pressure chamber in which it is preheated up to 600°C. The Mach number of the nozzle is 8, so that this temperature seems to be high enough to avoid air-condensation in the test chamber. The ejector is capable of reducing the back pressure to about

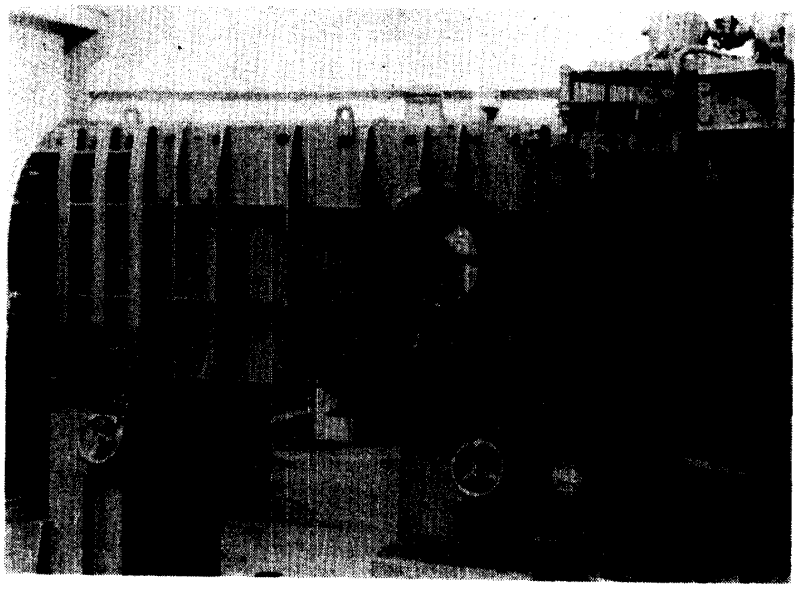

FIGURE 16. Wind tunnel.

0.1 atm. and the stagnation pressure is 50 kg/cm^2, so that the pressure ratio is high enought to start the wind tunnel. Duration of the wind tunnel is 120 sec..

5.3. *Model and Apparatus for Measurement*

The model used in the experiment consists of three parts; a nose-cone, a circular cylinder and a sting. A parablod-arc half-body of revolution with fineness ratio of 6.693 was used as a nose-cone. Sizes of the nose-cone are shown in Fig. 17 in

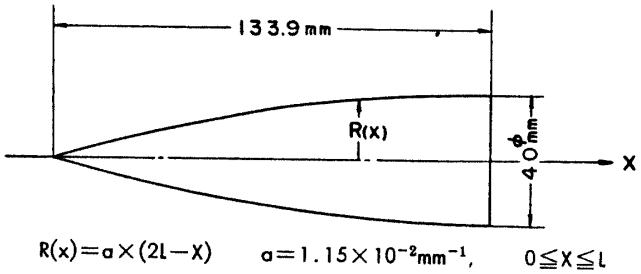

FIGURE 17. Size of nose-cone.

detail. The indicated fineness ratio is only a nominal one corresponding to geometric shape of the full-body of revolution. Therefore, the exact fineness ratio of the half-body of revolution used in the present experiment is 3.347. The nose-cone is made of stainless steel and has 9 pressure holes of 1$^{\phi}$ mm diameter set in the equal interval of 15 mm along a generating line.

A circular cylinder of 40$^{\phi}$ mm in diameter and 140 mm in length made of stainless steel was used as an after-body of the nose-cone. It was supported by a sting which was mounted on a strut downstream of the test chamber.

Static pressure on the nose-cone surface was measured by use of mercury manometers. The stagnation pressure was measured in the settling chamber by use of

a Bourdon-gauge together with a strain-gauge type pressure transducer for comparison. The stagnation temperature was also measured in the settling chamber by use of a thermocouple. Static pressure in the test chamber was not measured, because detailed measurement and calibration for the static pressure had already been made for each nozzle. Schlieren methnd was used for optical observation of shock wave at the tip of the model.

5.4. *Results and Discussion*

The ordinary supersonic experiment was carried out at stagnation pressures of 2 kg/cm^2 for $M=2$ and 5 kg/cm^2 for $M=3$, respectively. Therefore, the Reynolds numbers referred to length of the nose-cone are 3.27×10^6 for $M=2$ and 8.16×10^6 for $M=3$, respectively. The error in measurement of the surface pressure is within one percent.

Figs. 18a to 18b show schlieren photographs of the attached shock waves for Mach numbers of 2 and 3, respectively. Since the measurement of shock wave curvature at the tip from the schlieren photographs is very inaccurate, a comparison of the present theory with the experiment was made for the shock wave shape, which is shown in Fig. 19. The agreement between the results of the present theory and the experiment is found to be quite good.

In Figs. 20 and 21 are presented the measured surface pressure distributions for Mach numbers of 2 and 3, respectively. Results from the present theory and the method of characteristics are also shown for comparison. It must, however, be noted that no boundary layer correction was made for the theoretical results shown in Figs. 20 and 21, since boundary layer estimation revealed that the dis-

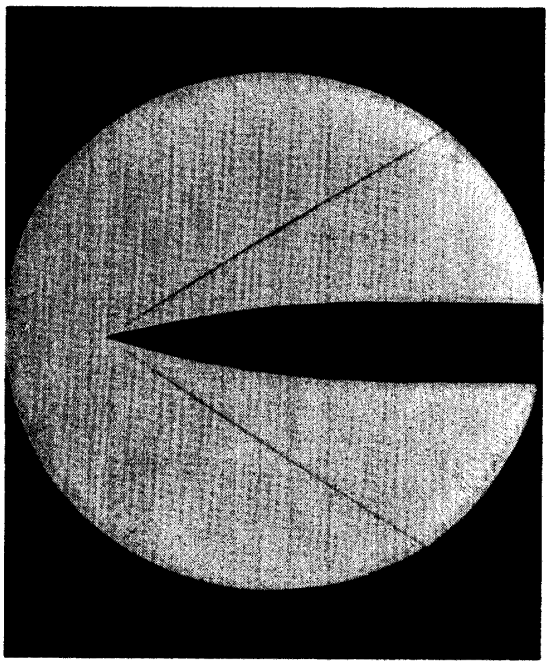

FIGURE 18a. Schliereh phtograph of shock wave, $M=2$, $\tau_0=0.1494$.

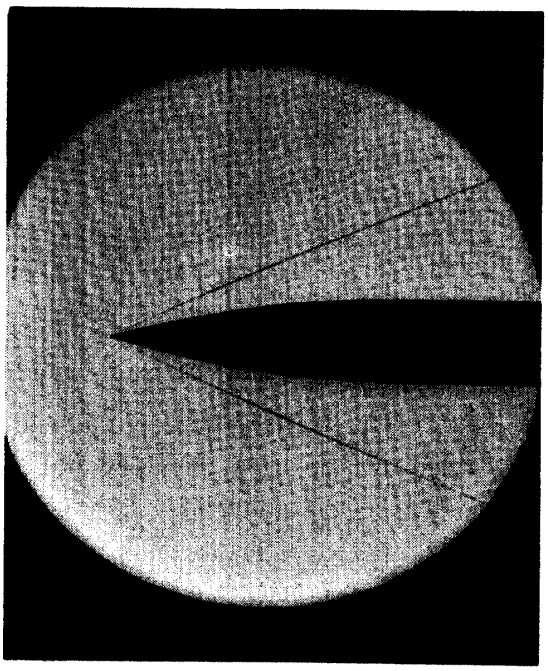

FIGURE 18b. Schileren photograph of shock wave, $M=3$, $\tau_0=0.1494$.

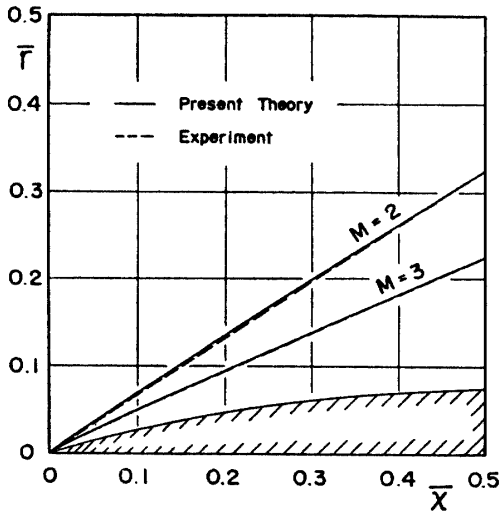

FIGURE 19. Comparison of the present theory with experiment for shock wave shape, $\tau_0=0.1494$.

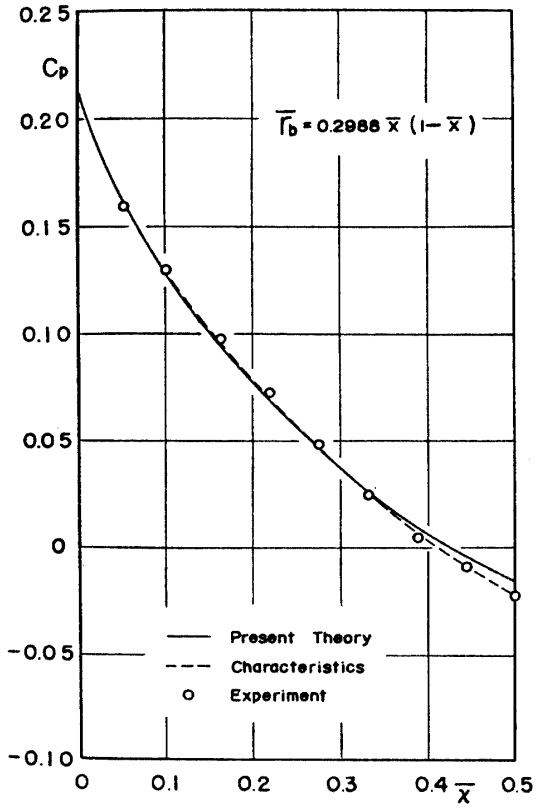

FIGURE 20. Surface pressure distribution on paraboloid-arc half-body of revolution, $M=2$, $\tau_0=0.1494$.

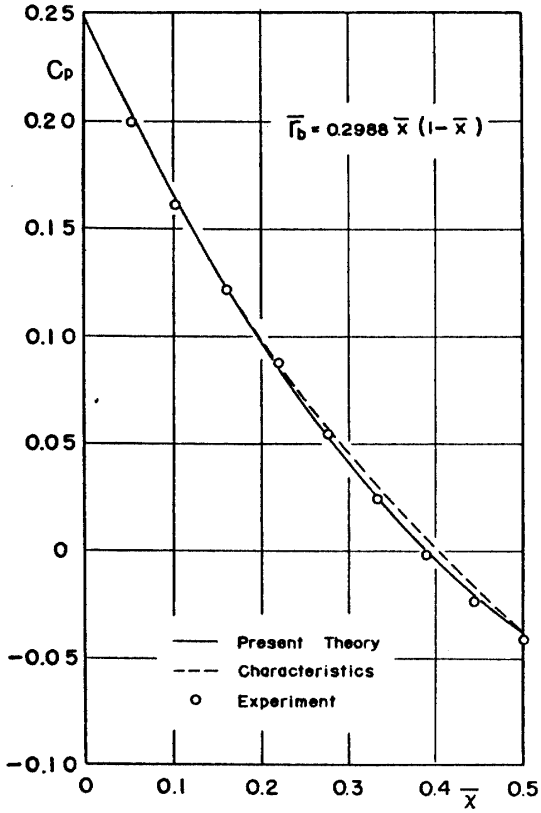

FIGURE 21. Surface pressure distribution on paraboloid-arc half-body of revolution, $M=3$, $\tau_0=0.1494$.

placement thickness on the body surface is thin enough to be negligible. For example, the relative error in pressure coefficient at the tip is only one percent.

As is seen in the figures, the present theory agrees well with the experimental data except for the very vicinity of $\bar{x}=0.5$, where it deviates slightly from the experiment. The method of characteristics, however, seems to agree well with

the experimental data for the entire surface of the nose-cone.

For the axially symmetric bodies with pointed tail the present approach indicates a singularity in expression for surface density, so that the pressure at the pointed tail is infinite. The same trend is also given in the linearized theory. From the experimental point of view, however, this infinite increase of the surface pressure is reduced to a finite increase due to separation of the boundary layer associated with interaction with the shock wave at the tail.

From the theoretical point of view, the slight deviation of the present theory from the experimental data and also from the method of characteristics near the smooth shoulder ($\bar{x}=0.5$) of the nose-cone is clearly due not to the essential inaccuracy of the present approach but to the lack of higher terms in series expansion of the stream function such as shown in Eq. (4.3.5) because of singular behaviour of the surface density near the pointed tail of the fullbody. Therefore, the deviation may be reduced by taking more terms with higher powers of x in series expansion of the stream function.

The hypersonic experiment was carried out at stagnation pressure of 49.5 kg/cm^2 and stagnation temperature of 510°C. Reynolds number referred to length of the nose-cone is 1.45×10^6. Relatively large stagnation temperature drop from the state in constant pressure chamber (600°C) is clearly due to conductive heat-loss through piping of the air passage. This stagnation temperature, however, is found to be high enough to avoid air-condensation in the test chamber at Mach number of 8.

Contrary to the ordinary supersonic case, the displacement thickness in this case of Mach number is not so thin that the effective change in body shape must be taken into consideration in order to compare the theoretical result with the experiment. However, the estimation of displacement thickness could not be done strictly, because surface temperature distribution of the model was not measured in the present experiment. For this reason it was roughly estimated by use of a result obtained for a $^3/_4$-power body of revolution with heat-insulated surface and for Prandtl rumber of unity, which is given in the form (12)

$$M\frac{\bar{\delta}^*}{\bar{x}}=\frac{0.6\bar{\chi}^{\frac{1}{2}}}{\left(1+\frac{\bar{r}_b}{\bar{\delta}^*}\right)^{\frac{1}{2}}}, \qquad \bar{\chi}=\frac{M^3\sqrt{C_\infty}}{\sqrt{Re_{x\infty}}} \tag{5.4.1}$$

where $\bar{\delta}^*$ and C_∞ denote displacement thickness and Chapman-Rubesin constant in free stream, respectively. Although the present model is not a $^3/_4$-power body of revolution, the displacement thickness may not so deviate from that calculated by use of Eq. (5.4.1). Thus, the effective shape of the body is obtained as

$$\bar{r}_b'=\bar{r}_b+\bar{\delta}^*=0.3237\bar{x}-0.3178\bar{x}^2+0.0870\bar{x}^3. \tag{5.4.2}$$

Fig. 22 shows effective body shape and corresponding theoretical shock wave shape at Mach number of 8. The original body shape and shock wave shape are also shown for comparison. As is seen in the figure, growth of radius of the effective body is about 26 percents at $\bar{x}=0.5$. Fig. 23 shows a schlieren photograph of

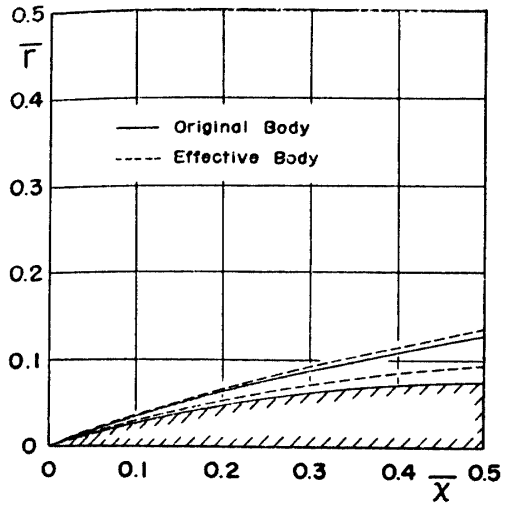

FIGURE 22. Effective body and shock wave shapes (present theory), $\tau_0 = 0.1494$, $M=8$.

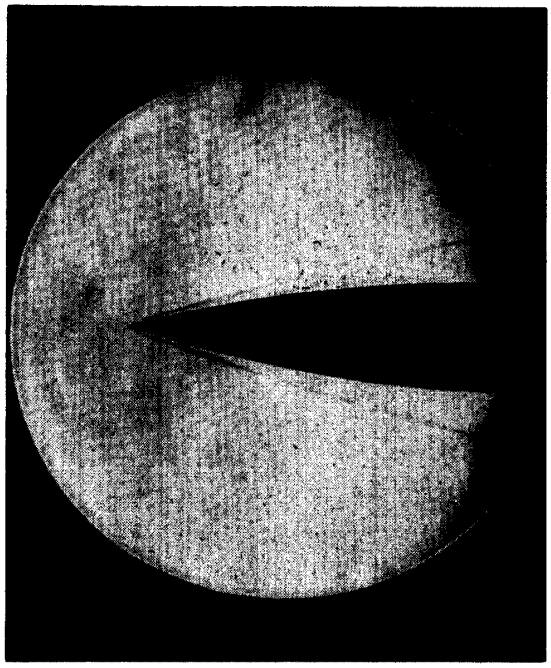

FIGURE 23. Schileren photograph of shock wave, $M=8$, $\tau_0=0.1494$.

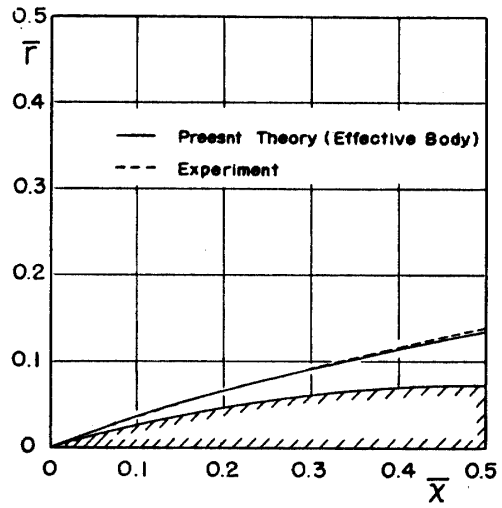

FIGURE 24. Comparison of the present theory with experiment for shock wave shape (effective body), $M=8$, $\tau_0=0.1494$.

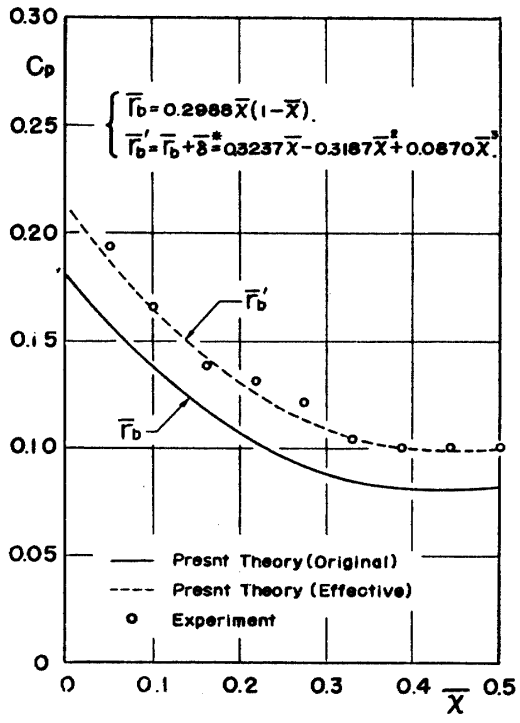

FIGURE 25. Surface pressure distribution on paraboloid-arc half-body of revolution, $M=8$, $\tau_0=0.1494$.

shock wave at $M=8$, which is replotted in Fig. 24 together with the theoretical result for the effective body for comparison. The agreement is found to be quite good. In Fig. 25 is presented the measured pressure distribution on a paraboloid-arc half-body of revolution at $M=8$. The theoretical pressure distributions are

also shown in the same figure for comparison. The full line indicates pressure on original body, which deviates far from the experimental data on the entire surface. On the other hand, the broken line indicates the present theory applied to the effective body, which is found to be fairly in good agreement with the experiment on the entire surface of the body.

6. Conclusion

A second-order supersonic small disturbance theory has been developed for plane and axially symmetric flows involving shock waves, laying an emphasis on the extension of Van Dyke's first-order hypersonic small disturbance theory to comparatively low Mach numbers and thick bodies.

A set of figures has been presented giving the initial ratio of shock wave to body curvature, initial gradient of surface pressure for Mach numbers of 2, 3 and 5, and for a fairly wide range of semi-vertex angle of the body. Several examples for surface pressure distribution on biconvex circular-arc airfoils and a paraboloid-arc half-body of revolution have been also presented and compared with the method of characteristics, shock-expansion method and other approximate method when available.

It has been shown that the present theory agrees well with the method of characteristics for both plane and axially symmetric convex bodies with semi-vertex angle up to 15° and for Mach numbers up to 5.

Experimental measurement for the surface pressure on a paraboloid-arc half-body of revolution with nominal fineness ratio of 6.693 was made for Mach numbers of 2, 3 and 8, and the results were compared with the present theory and the method of characteristics. It has been found that the present theory agrees well with the experiment. Comparison of calculated shapes of shock wave with schlieren photographs has also confirmed this.

Acknowledgement

Author wishes to express his gratitude to Profs. R. Kawamura and H. Oguchi for their valuable advices and discussions upon this work. The author is also very grateful to Prof. I. Tani for his kind advices.

Department of Aerodynamics
Institute of Space and Aeronautical Science
University of Tokyo, Tokyo.
September 25, 1964

References

[1] Heaslet, N. A. and Lomax, H.: The Use of Source-Sink and Doublet Distributions Extended to the Solution of Boundary Value Problems in Supersonic Flow. NACA Rep., No. 900, 1948.

[2] Ward, G. N.: Supersonic Fow Past Slender Pointed Bodies. Quart. Jour. Mech. and Appl. Math., Vol. 2, 1949.
[3] Lighthill, M. J.: Two-Dimensional Supersonic Airfoil Theory. Rep. Memor. Aero. Res. Coun. No. 1929, 1944.
[4] Van Dyke, M. D.: Practical Calculation of Second-Order Supersonic Flow Past Nonlifting Bodies of Revolution. NACA TN 2744, 1952.
[5] Eggers, Jr. A. J. and Syvertson, C. A.: Inviscid Fow About Airfoils at High Supersonic Speeds. NACA TN 2646, 1952.
[6] Kraus, S.: An Analysis of Supersonic Flow in the Region of the Leading Edge of Curued Airfoils, Including Charts for Determining Surface-Pressure Gradient and Shock-Wave Curvature. NACA TN 2729, 1952.
[7] Shen, S. F. and Lin, C. C.: On the Attached Curved Shock in Front of a Sharp-Nosed Axially Symmetric Body Placed in a Uniform Stream. NACA TN 2505, 1951.
[8] Van Dyke, M. D.; A Study of Hypersonic Small-Disturbance Theory. NACA Tep. 1194, 1954.
[9] Van Dyke, M. D.: The Combined Supersonic-Hypersonic Similarity Rule. Jour. Aero. Sci. Vol. 18, No. 7, 1951.
[10] Ames Research Staff: Equations, Tables and Charts for Compressible Fow. NACA Rep. 1135, 1947.
[11] Taylor, G. I. and Maccoll, J. W.: The Air Pressure Over a Cone Moving at High Speeds. Proc. Roy. Soc. (London), A, Vol. 139, No. 838, 1933.
[12] Hayes, W. D. and Probstein, R. F.: Hypersonic Flow Theory. Academic Press, New York and London, 1959.

Appendix 1.

Initial ratio of shock wave to body curvature given by Kraus [6] has a form

$$\frac{K_s}{K_b}=\frac{\gamma+1}{4\cos(\beta-\theta)}\left[\frac{1-\dfrac{\tan^2(\beta-\theta)}{\tan^2\mu_2}}{\dfrac{\tan^2(\beta-\theta)}{\tan^2\mu_2}+\dfrac{1}{2}\left\{\dfrac{\cos^2\mu_2}{\cos^2(\beta-\theta)}+\dfrac{1}{M^2\sin^2\beta}\right\}}\right], \tag{A.1.1}$$

where β, θ and μ_2 denote initial shock wave angle, semi-vertex angle of the airfoil and Mach wave angle just behind the shock wave, respectively. Numerator in bracket of the above equation can be written by use of shock wave relation as

$$1-\frac{\tan^2(\beta-\theta)}{\tan^2\mu_2}=\frac{\dfrac{\gamma+1}{2}(M^2\sin^2\beta-1)}{\cos^2(\beta-\theta)\left(\gamma M^2\sin^2\beta-\dfrac{\gamma-1}{2}\right)},$$

which is further simplified as

$$1-\frac{\tan^2(\beta-\theta)}{\tan^2\mu_2}\doteqdot\frac{1}{\gamma}\left(\frac{\gamma+1}{2}\right)^2\frac{1}{\cos^2(\beta-\theta)}\frac{\delta}{\tau}, \tag{A.1.2}$$

where has been used an approximate expression such as

$$M^2\tau^2-(1+\tau^2)\doteqdot\frac{\gamma+1}{2}M^2\tau\delta, \qquad \tau=\tan\beta, \qquad \delta=\tan\theta.$$

Moreover, since

$$\frac{\cos^2\mu_2}{\cos^2(\beta-\theta)}=\frac{\tan^2(\beta-\theta)}{\tan^2\mu_2}\,\frac{2\gamma M^2\sin^2\beta-(\gamma-1)}{(\gamma-1)M^2\sin^2\beta+2},$$

so that the denominator in bracket of Eq. (A.1.1) may be of order of unity and $\cos(\beta-\theta)$ is also of order of unity for small value of δ. Therefore, initial ratio of shock wave to body curvature may have an order

$$\frac{K_s}{K_b}=0\left(\frac{\delta}{\tau}\right). \tag{A.1.3}$$

Appendix 2.

From Eq. (3.4.2), ψ_r and ψ_x are given, respectively, as

$$\begin{aligned}\psi_r&=f'(\theta)-lxg'(\theta)-x^2\{mh'(\theta)+l^2i'(\theta)\}-\cdots\cdot\\ \psi_x&=f(\theta)-\theta f'(\theta)-lx\{2g(\theta)-\theta g'(\theta)\}\\ &\quad-x^2[m\{3h(\theta)-\theta h'(\theta)\}+l^2\{3i(\theta)-\theta i'(\theta)\}]-\cdots\cdot\end{aligned} \tag{A.2.1}$$

At the shock wave the conical parameter is written as

$$\theta_s=1-\frac{1}{2}lx-\frac{1}{3}mx^2-\cdots\cdot$$

Taylor expansion of ψ_r and ψ_x at the shock wave has the forms

$$\begin{aligned}(\psi_r)_s&=\bar{A}_0-lxg'(1)-x^2\left[mh'(1)+l^2\left\{i'(1)-\frac{1}{2}g''(1)\right\}\right]-\cdots\cdot\\ (\psi_x)_s&=-\bar{B}_0-lx\{2g(1)-g'(1)\}-x^2\left[m\{3h(1)-h'(1)\}\right.\\ &\quad\left.+l^2\left\{3i(1)-i'(1)-\frac{1}{2}g'(1)+\frac{1}{2}g''(1)\right\}\right]-\cdots\cdot\end{aligned} \tag{A.2.2}$$

Comparison of Eq. (A.2.2) with Eq. (3.4.4a) also gives

$$\begin{aligned}g'(1)&=-\bar{A}_1\\ h'(1)&=-\bar{A}_1\\ i(1)&=\frac{1}{2}g''(1)-\bar{A}_2\end{aligned} \tag{A.2.3}$$

and comparison of Eq. (A.2.2) with Eq. (3.4.4b) also gives

$$\begin{aligned}2g(1)-g'(1)&=\bar{B}_1\\ 3h(1)-h'(1)&=\bar{B}_1\\ 3i(1)-i'(1)-\frac{1}{2}g'(1)+\frac{1}{2}g''(1)&=\bar{B}_2\end{aligned} \tag{A.2.4}$$

Hence,

$$\begin{aligned}g(1)&=\frac{1}{2}\left\{g'(1)+\bar{B}_1\right\}=-\frac{1}{2}\bar{B}_0\\ h(1)&=\frac{1}{3}\left\{h'(1)+\bar{B}_1\right\}=-\frac{1}{3}\bar{B}_0\end{aligned} \tag{A.2.5}$$

$$i(1)=\frac{1}{3}\left\{i'(1)+\frac{1}{2}g'(1)-\frac{1}{2}g''(1)+\bar{B}_2\right\}$$
$$=\frac{1}{3}\left(\bar{B}_2-\bar{A}_2-\frac{1}{2}\bar{A}_1\right)$$

NOTE

Order estimation may reveal that the term of $\tau^2\omega'\psi_r^{\tau+1}\psi_x^2$ in Eq. (3.1.12) is of order of δ^3/τ and, consequently, negligible from the basic assumption. However, it was particularly retained in the present approach as the leading term of $\tau^2\omega'\rho^{\tau+1}\psi_x^2$ in Eq. (3.1.3). Such a retention may be acceptable in the sense that it does not disturb the accuracy of the present theory.

The same is true for retaining the term of $\tau^2\frac{1}{r^{\tau-1}}\omega'\psi_r^{\tau+1}\psi_x^2$ in Eq. (4.1.7) for axially symmetric flows.